elevated *RTL1* expression.[2] Indeed, DLK1 protein expression was not exaggerated in case 3 with typical upd(14)pat phenotype, and DIO3 protein expression was not enhanced in cases 1–3. It may be possible, however, that the abnormality of placental structures may have resulted in a difference in immunostaining without an actual change in gene expression. This point awaits further investigations.

Third, villous chorangiosis, stromal expansion, and mesenchymal dysplasia were not identified in the placental samples of cases 1–3, although such a lesion(s) may have existed in non-examined portions. Notably, such lesions are frequently observed in placentas of patients with BWS.[19-21] Thus, while both upd(14)pat and BWS are associated with placentomegaly and polyhydroamnios, characteristic histological findings appear to be different between upd(14)pat and BWS.

This study would also provide useful information on the methylation patterns of the *MEG3*-DMR in the placenta. Our previous studies using formalin-fixed and paraffin-embedded placental samples revealed that roughly two-thirds of clones were hypermethylated and the remaining roughly one-third of clones were hypomethylated in case 3 as well as in the previously reported patients with upd(14)pat (not cases 1 and 2) and epimutation (hypermethylation of the IG-DMR and the *MEG3*-DMR of maternal origin), and that roughly one-third of clones were hypermethylated and the remaining roughly two-thirds of clones were hypomethylated in control placental samples (see Fig. S2C in ref. 2). However, this study showed that the *MEG3*-DMR was grossly hypomethylated in the fresh placental samples of cases 1 and 2, with an extent similar to that identified in the fresh control placental samples. In this regard, it is notable that PCR products could be obtained only after 35 cycles for the formalin-fixed and paraffin-embedded placental samples and were sufficiently obtained after 30 cycles for the fresh placental samples. Thus, several specific clones may have been selectively amplified in the previous study. Furthermore, it may be possible that efficacy of bisulfite treatment (conversion of unmethylated cytosine into uracils and subsequently thymines) may be insufficient for the formalin-fixed and paraffin-embedded placental samples. Thus, it appears that the present data denote precise methylation patterns of the *MEG3*-DMR in the placenta.

In summary, the present study provides useful clues for the clarification of regulatory mechanism for the *RTL1* expression, imprinting status of *DIO3* and characteristic placental histological findings in patients with upd(14)pat and related conditions. Further studies will help improve our knowledge about upd(14)pat and related conditions.

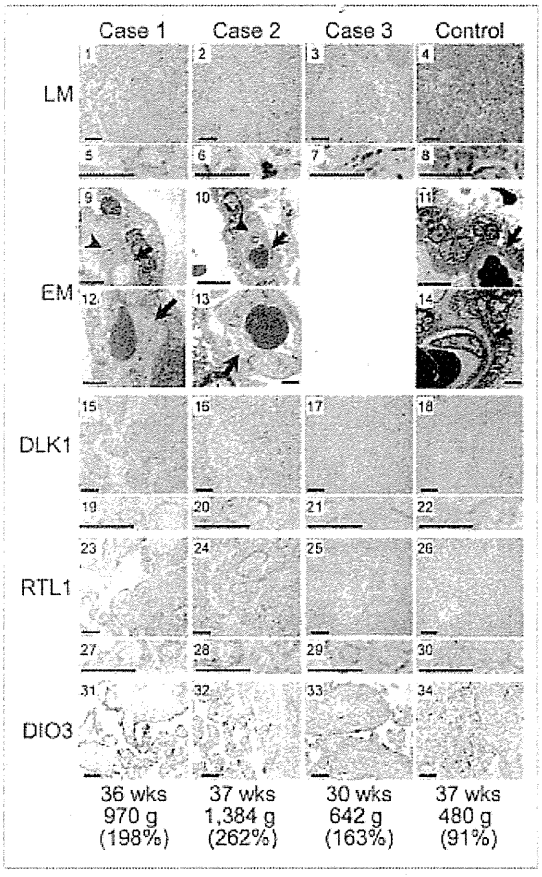

Figure 5. Histological examinations. LM, light microscopic examinations; EM, electron microscopic examinations; DLK1, RTL1 and DIO3, immunohistochemical examinations for the corresponding proteins. The arrows and arrowheads in the EM findings indicate endothelial cells and pericytes, respectively. Scale bars represent 100 μm for 1–4, 15–18, 23–26 and 31–34, 50 μm for 5–8, 19–22 and 27–30, 5 μm for 9–11 and 2 μm for 12–14. Gestational age, placental weight, and % placental weight assessed by the gestational age-matched Japanese references for placental weight[4,22] are described.

Methods

Ethical approval. This study was approved by the Institutional Review Board Committees of each investigator, and performed after obtaining written informed consent.

Primers. Primers utilized in this study are summarized in **Table S3**.

Sample preparation for molecular studies. Genomic DNA samples were obtained from leukocytes using FlexiGene DNA Kit (Qiagen) and from placental samples using ISOGEN (Nippon Gene). Transcripts of *DLK1*, *MEG3*, *RTL1*, *MEG8* and *DIO3* were isolated with ISOGEN (Nippon Gene), and *microRNAs* were extracted with mirVana™ miRNA Isolation Kit (Ambion). After DNase treatment, cDNA samples for *DLK1*, *MEG3*, *MEG8* and *DIO3* were prepared with oligo(dT) primers from 1 μg of RNA using Superscript III Reverse Transcriptase (Invitrogen), and those of *microRNAs* were synthesized from 300 ng of RNA using TaqMan MicroRNA Reverse Transcription Kit (Applied Biosystems). For *RTL1*, 3'-RACE was utilized to prevent amplification of *RTL1as*; cDNA was synthesized from 1 μg of RNA using Superscript III Reverse Transcriptase with a long primer hybridizing to poly A site and introducing the adaptor sequence. Lymphocyte metaphase spreads for FISH analysis were prepared from leukocytes using colcemide (Invitrogen).

Molecular studies. Microsatellite analysis for 19 loci on chromosome 14, methylation analysis for the IG-DMR and

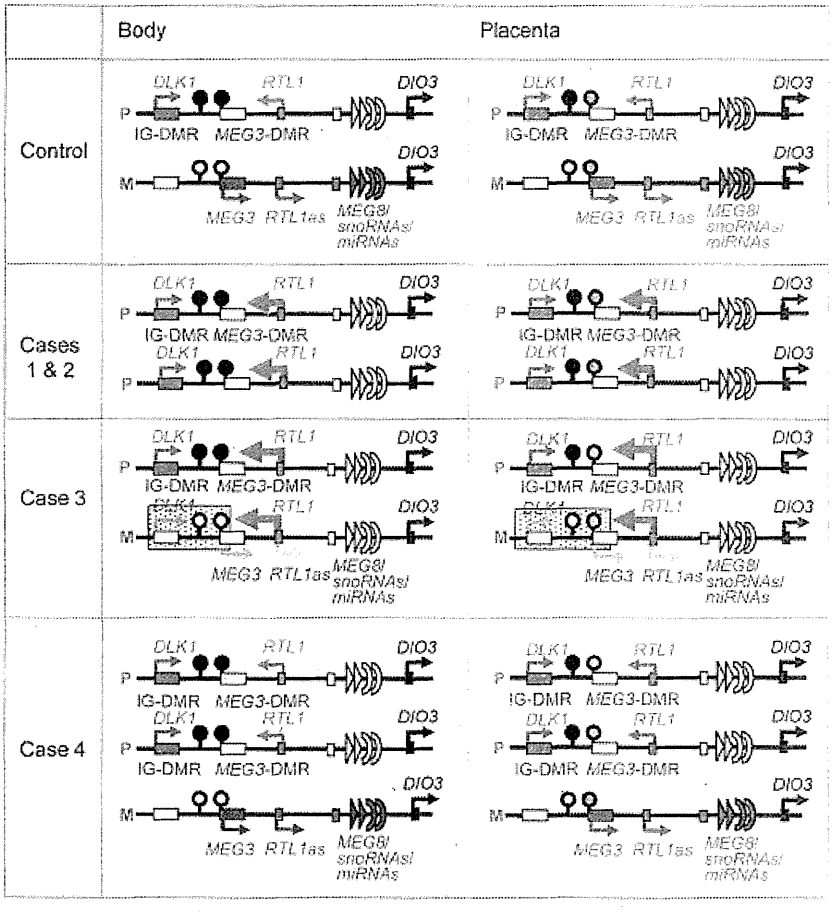

Figure 6. Schematic representation of the chromosome 14q32.2 imprinted region in a control subject, cases 1 and 2 with upd(14)pat, case 3 with a microdeletion (indicated by stippled rectangles), and case 4 with two copies of the imprinted region of paternal origin and a single copy of the imprinted region of maternal origin. This figure has been constructed using the present results and the previous data.[2,3] P, paternally derived chromosome; M, maternally derived chromosome. Filled and open circles represent hypermethylated and hypomethylated DMRs, respectively; since the *MEG3*-DMR is grossly hypomethylated and regarded as non-DMR in the placenta, it is painted in gray. *PEGs* (*DLK1* and *RTL1*) are shown in blue, *MEGs* (*MEG3*, *RTL1as*, *MEG8*, *snoRNAs* and *miRNAs*) in red, a probably non-imprinted gene (*DIO3*) in black, and non-expressed genes in white. Thick arrows for *RTL1* in cases 1–3 represent increased *RTL1* expression that is ascribed to loss of functional microRNA-containing *RTL1as* as a repressor for *RTL1*.

the *MEG3*-DMR, and FISH analyses for the 14q32.2 region were performed as described previously.[2,3] For FISH analysis of 17p13.3, a 17p sub-telomere probe and an RP11–411G7 probe for the 17p13.3 region were utilized, together with a CEP17 probe for the 17p11.1 region utilized as an internal control. The 17p sub-telomere probe was detected according to the manufacture's protocol, the RP11–411G7 probe was labeled with digoxigenin and detected by rhodamine anti-digoxigenin, and the CEP17 control probe was labeled with biotin and detected by avidin conjugated to fluorescein isothiocyanate. Quantitative real-time PCR analysis was performed on an ABI PRISM 7000 (Applied Biosystems) using TaqMan real-time PCR probe primer mixture for the following genes (assay No: Hs00171584 for *DLK1*, Hs00292028 for *MEG3*, Hs00419701 for *MEG8* and Hs00704811 for *DIO3*; assay ID: 001028 for *miR433* and 000452 for *miR127*). For *RTL1*, q-PCR analysis was performed with a forward primer hybridized to the sequence of *RTL1* and a reverse primer hybridized to the adaptor sequence. Fifty nanongrams of cDNA in a 50 μl reaction mixture contacting 2× KOD FX buffer (Toyobo), 2.0 mM dNTP mixture (Toyobo), KOD FX (Toyobo), SYBR Green I (Invitrogen), and primer set for *RTL1* were subjected to the ABI PRISM 7000. Data were normalized against *GAPDH* (catalog No: 4326317E) for *DLK1*, *MEG3*, *MEG8*, *RTL1*, and *DIO3*, and against *RNU48* (assay ID: 0010006) for *microRNAs*. The expression studies were performed three times for each sample. Oligoarray CGH was performed using 1× 1M format Human Genome Array (Catalog No G4447A) (Agilent Technologies).

Histopathogical analysis. Placental samples were fixed with 20% buffered formaldehyde at room temperature and embedded in paraffin wax according to standard protocols for LM examinations. Then, sections of 3 μm thick were stained with hematoxylin-eosin. For EM examinations, fresh placental tissues were fixed with phosphate-buffered 2.5% glutaraldehyde, postfixed in 1% osmium tetroxide, and embedded in Epon 812 (catalog No. R3245, TAAB). Semithin sections were stained with 1% methylene blue, and ultrathin sections were double-stained with uranyl acetate and lead citrate. Subsequently, they were examined with a Ninhon Denshi JEM-1230 electron microscope.

For IHC analysis, sections of 3 μm thick were prepared by the same methods utilized for the LM examinations, and were examined with rabbit anti human DLK1 polyclonal antibody at 1:100 dilutions (catalog No 10636-1-AP, ProteinTech Group), rabbit anti human RTL1 polyclonal antibody at 1:200 dilutions, and rabbit anti human DIO3 polyclonal antibody at 1:50 dilutions (catalog No ab102926, abcam); anti human RTL1 polyclonal antibody was produced by immunizing rabbits with the synthesized RTL1 peptide (NH2-RGFPRDPSTESG-COOH) in this study. Sections were dewaxed in xylene and rehydrated through graded ethanol series and, subsequently, incubated in 10% citrate buffer (pH 6.0) for 40 min in a 98°C water bath, for antigen retrieval. Endogenous peroxidase activity was quenched with 1% H_2O_2 and 100% methanol for 20 min. To prevent non-specific background staining, sections are incubated with Protein Block Serum-Free (Dako corporation) for 10 min at room temperature. Then, sections were incubated overnight with primary antibody at 4°C

and, subsequently, treated with the labeled polymer prepared by combining amino acid polymers with peroxidase and anti-rabbit polyclonal antibody (Histofine Simple Stain MAX PO MULTI, Nichirei). Peroxidase activities were visualized by diaminobenzidine staining, and the nuclei were stained with hematoxylin.

Disclosure of Potential Conflicts of Interest

No potential conflicts of interest were disclosed.

Acknowledgments

This work was supported by Grants-in-Aid for Scientific Research (A) (22249010) and Research (B) (21028026) from the Japan Society for the Promotion of Science (JSPS), by Grants-in-Aid for Scientific Research on Innovative Areas (22132004-A04) from the Ministry of Education, Culture, Sports, Science and Technology (MEXT), by Grants for Research on Intractable Diseases (H22–161) from the Ministry of Health, Labor and Welfare (MHLW), by Grant for National Center for Child Health and Development (23A-1), and by Grant from Takeda Science Foundation and from Novartis Foundation.

Supplemental Materials

Supplemental materials may be found here:
www.landesbioscience.com/journals/epigenetics/article/21937

References

1. da Rocha ST, Edwards CA, Ito M, Ogata T, Ferguson-Smith AC. Genomic imprinting at the mammalian Dlk1-Dio3 domain. Trends Genet 2008; 24:306-16; PMID:18471925; http://dx.doi.org/10.1016/j.tig.2008.03.011.
2. Kagami M, Sekita Y, Nishimura G, Irie M, Kato F, Okada M, et al. Deletions and epimutations affecting the human 14q32.2 imprinted region in individuals with paternal and maternal upd(14)-like phenotypes. Nat Genet 2008; 40:237-42; PMID:18176563; http://dx.doi.org/10.1038/ng.2007.56.
3. Kagami M, O'Sullivan MJ, Green AJ, Watabe Y, Arisaka O, Masawa N, et al. The IG-DMR and the MEG3-DMR at human chromosome 14q32.2: hierarchical interaction and distinct functional properties as imprinting control centers. PLoS Genet 2010; 6:e1000992; PMID:20585555; http://dx.doi.org/10.1371/journal.pgen.1000992.
4. Kagami M, Yamazawa K, Matsubara K, Matsuo N, Ogata T. Placentomegaly in paternal uniparental disomy for human chromosome 14. Placenta 2008; 29:760-1; PMID:18619672; http://dx.doi.org/10.1016/j.placenta.2008.06.001.
5. Lin SP, Youngson N, Takada S, Seitz H, Reik W, Paulsen M, et al. Asymmetric regulation of imprinting on the maternal and paternal chromosomes at the Dlk1-Gtl2 imprinted cluster on mouse chromosome 12. Nat Genet 2003; 35:97-102; PMID:12937418; http://dx.doi.org/10.1038/ng1233.
6. Sekita Y, Wagatsuma H, Nakamura K, Ono R, Kagami M, Wakisaka N, et al. Role of retrotransposon-derived imprinted gene, Rtl1, in the feto-maternal interface of mouse placenta. Nat Genet 2008; 40:243-8; PMID:18176565; http://dx.doi.org/10.1038/ng.2007.51.
7. Lage JM. Placentomegaly with massive hydrops of placental stem villi, diploid DNA content, and fetal omphaloceles: possible association with Beckwith-Wiedemann syndrome. Hum Pathol 1991; 22:591-7; PMID:1864589; http://dx.doi.org/10.1016/0046-8177(91)90237-J.
8. Yamazawa K, Kagami M, Nagai T, Kondoh T, Onigata K, Maeyama K, et al. Molecular and clinical findings and their correlations in Silver-Russell syndrome: implications for a positive role of IGF2 in growth determination and differential imprinting regulation of the IGF2-H19 domain in bodies and placentas. J Mol Med (Berl) 2008; 86:1171-81; PMID:18607558; http://dx.doi.org/10.1007/s00109-008-0377-4.
9. Georgiades P, Watkins M, Burton GJ, Ferguson-Smith AC. Roles for genomic imprinting and the zygotic genome in placental development. Proc Natl Acad Sci U S A 2001; 98:4522-7; PMID:11274372; http://dx.doi.org/10.1073/pnas.081540898.
10. Fowden AL, Sibley C, Reik W, Constancia M. Imprinted genes, placental development and fetal growth. Horm Res 2006; 65(Suppl 3):50-8; PMID:16612114; http://dx.doi.org/10.1159/000091506.
11. Georgiades P, Ferguson-Smith AC, Burton GJ. Comparative developmental anatomy of the murine and human definitive placentae. Placenta 2002; 23:3-19; PMID:11869088; http://dx.doi.org/10.1053/plac.2001.0738.
12. Tsai CE, Lin SP, Ito M, Takagi N, Takada S, Ferguson-Smith AC. Genomic imprinting contributes to thyroid hormone metabolism in the mouse embryo. Curr Biol 2002; 12:1221-6; PMID:12176332; http://dx.doi.org/10.1016/S0960-9822(02)00951-X.
13. Yamanaka M, Ishikawa H, Saito K, Maruyama Y, Ozawa K, Shibasaki J, et al. Prenatal findings of paternal uniparental disomy 14: report of four patients. Am J Med Genet A 2010; 152A:789-91; PMID:20186803; http://dx.doi.org/10.1002/ajmg.a.33247.
14. Suzumori N, Ogata T, Mizutani E, Hattori Y, Matsubara K, Kagami M, et al. Prenatal findings of paternal uniparental disomy 14: Delineation of further patient. Am J Med Genet A 2010; 152A:3189-92; PMID:21108407; http://dx.doi.org/10.1002/ajmg.a.33719.
15. Kagami M, Kato F, Matsubara K, Sato T, Nishimura G, Ogata T. Relative frequency of underlying genetic causes for the development of UPD(14)pat-like phenotype. Eur J Hum Genet 2012; 20:928-32; PMID:22353941; http://dx.doi.org/10.1038/ejhg.2012.26.
16. Seitz H, Youngson N, Lin SP, Dalbert S, Paulsen M, Bachellerie JP, et al. Imprinted microRNA genes transcribed antisense to a reciprocally imprinted retrotransposon-like gene. Nat Genet 2003; 34:261-2; PMID:12796779; http://dx.doi.org/10.1038/ng1171.
17. Davis E, Caiment F, Tordoir X, Cavaillé J, Ferguson-Smith A, Cockett N, et al. RNAi-mediated allelic trans-interaction at the imprinted Rtl1/Peg11 locus. Curr Biol 2005; 15:743-9; PMID:15854907; http://dx.doi.org/10.1016/j.cub.2005.02.060.
18. Köhrle J. Thyroid hormone transporters in health and disease: advances in thyroid hormone deiodination. Best Pract Res Clin Endocrinol Metab 2007; 21:173-91; PMID:17574002; http://dx.doi.org/10.1016/j.beem.2007.04.001.
19. Kraus FT, Redline RW, Gersell DJ, Nelson DM, Dicker JM. Disorders of placental Development. Placental Pathology (Atlas of Noutumor Pathology). Washington, DC: American Registry of Pathology, 2004:59-68.
20. Fox HE, Sebire NJ. The placenta in abnormalities and disorders of the fetus. Pathology of the Placenta. Third edition, Philadelphia, PA: SAUNDERS, 2007:262-3.
21. Parveen Z, Tongson-Ignacio JE, Fraser CR, Killeen JL, Thompson KS. Placental mesenchymal dysplasia. Arch Pathol Lab Med 2007; 131:131-7; PMID:17227114.
22. Nakayama M. Placental pathology. Tokyo, Igaku Shoin, 2002:106-7 (in Japanese).

Mamld1 Deficiency Significantly Reduces mRNA Expression Levels of Multiple Genes Expressed in Mouse Fetal Leydig Cells but Permits Normal Genital and Reproductive Development

Mami Miyado, Michiko Nakamura, Kenji Miyado, Ken-ichirou Morohashi, Shinichiro Sano, Eiko Nagata, Maki Fukami, and Tsutomu Ogata

Departments of Molecular Endocrinology (M.M., M.N., M.F., T.O.) and Reproductive Biology (K.Mi.), National Research Institute of Child Health and Development, Tokyo 157-8535, Japan; Department of Molecular Biology (K.Mo.), Graduate School of Medical Sciences, Kyushu University, Fukuoka 812-8582, Japan; and Department of Pediatrics (S.S., E.N., T.O.), Hamamatsu University School of Medicine, Hamamatsu 431-3192, Japan

Although mastermind-like domain containing 1 (*MAMLD1*) (*CXORF6*) on human chromosome Xq28 has been shown to be a causative gene for 46,XY disorders of sex development with hypospadias, the biological function of *MAMLD1/Mamld1* remains to be elucidated. In this study, we first showed gradual and steady increase of testicular *Mamld1* mRNA expression levels in wild-type male mice from 12.5 to 18.5 d postcoitum. We then generated *Mamld1* knockout (KO) male mice and revealed mildly but significantly reduced testicular mRNA levels (65–80%) of genes exclusively expressed in Leydig cells (*Star*, *Cyp11a1*, *Cyp17a1*, *Hsd3b1*, and *Insl3*) as well as grossly normal testicular mRNA levels of genes expressed in other cell types or in Leydig and other cell types. However, no demonstrable abnormality was identified for cytochrome P450 17A1 and 3β-hydroxysteroid dehydrogenase (HSD3B) protein expression levels, appearance of external and internal genitalia, anogenital distance, testis weight, Leydig cell number, intratesticular testosterone and other steroid metabolite concentrations, histological findings, *in situ* hybridization findings for *sonic hedgehog* (the key molecule for genital tubercle development), and immunohistochemical findings for anti-Müllerian hormone (Sertoli cell marker), HSD3B (Leydig cell marker), and DEAD (Asp-Glu-Ala-Asp) box polypeptide 4 (germ cell marker) in the KO male mice. Fertility was also normal. These findings imply that *Mamld1* deficiency significantly reduces mRNA expression levels of multiple genes expressed in mouse fetal Leydig cells but permits normal genital and reproductive development. The contrastive phenotypic findings between *Mamld1* KO male mice and *MAMLD1* mutation positive patients would primarily be ascribed to species difference in the fetal sex development. (***Endocrinology*** **153: 6033–6040, 2012)**

Mastermind-like domain containing 1 (*MAMLD1*) (alias *CXORF6*) on human chromosome Xq28 is a causative gene for 46,XY disorders of sex development (DSDs) with hypospadias as a salient clinical phenotype. Indeed, several pathologic nonsense and frameshift mutations (p.E124X, p.Q197X, p.R653X, and p.E109fsX121) have been identified in patients with various types of hypospadias with and without other associated genital abnormalities, such as micropenis and cryptorchidism (1–3). In addition, a specific polymorphism(s) and a haplotype of *MAMLD1* appear to constitute a genetic risk factor for hypospadias (2, 4, 5).

To date, several important findings have been revealed for *MAMLD1* and its mouse homolog *Mamld1*. First, the

ISSN Print 0013-7227 ISSN Online 1945-7170
Printed in U.S.A.
Copyright © 2012 by The Endocrine Society
doi: 10.1210/en.2012-1324 Received March 21, 2012. Accepted September 20, 2012.
First Published Online October 18, 2012

Abbreviations: Ab, Antibody; AGD, anogenital distance; AGI, AGD index; CYP17A1, cytochrome P450 17A1; dpc, days postcoitum; DSD, disorder of sex development; HSD3B, 3β-hydroxysteroid dehydrogenase; KO, knockout; *MAMLD1*, mastermind-like domain containing 1; MLTC, mouse Leydig tumor cell; *Shh*, *sonic hedgehog*; siRNA, small interfering RNA; T, testosterone; WT, wild type.

upstream region of *MAMLD1/Mamld1* harbors a putative binding site for *NR5A1* (alias *SF-1* and *AD4BP*) (6) that regulates the transcription of a vast array of genes involved in sex development (7). Second, nuclear receptor subfamily 5, group A, member 1 protein can bind to the putative target site and exert a transactivation function for *Mamld1* (6). Third, *Mamld1* is clearly coexpressed with mouse *Nr5a1* in fetal Leydig and Sertoli cells in the fetal testis (1). Fourth, transient *Mamld1* knockdown using small interfering RNAs (siRNAs) significantly reduces *Cyp17a1* expression (8) and testosterone (T) production in cultured mouse Leydig tumor cells (MLTCs) (6, 8). These findings imply that *MAMLD1/Mamld1* is involved in the molecular network for T production probably via the transactivation of *CYP17A1/Cyp17a1* under the regulation of *NR5A1* and that *MAMLD1* mutations result in 46,XY DSD phenotype with hypospadias primarily because of compromised, but not abolished, T production around the critical period for sex development.

However, the biological function of *MAMLD1/Mamld1* during testis development remains to be elucidated. Thus, we examined testicular *Mamld1* mRNA expression pattern in wild-type (WT) male mice and performed molecular and phenotypic analyses in *Mamld1* knockout (KO) male mice.

Materials and Methods

WT and *Mamld1* KO male mice

We examined WT male mice of the C57BL/6 strain purchased from Sankyo Labo Service Corp., Inc. (Tokyo, Japan) and *Mamld1* KO male mice generated by Macrogen, Inc. (Seoul, Korea). This study was approved by the Animal Ethics Committee of National Research Institute for Child Health and Development.

Mamld1 KO male mice were produced by a standard gene-targeting procedure (9). In brief, a targeting vector was designed to replace *Mamld1* exon 3, which harbors a translation start codon and approximately two thirds of the coding sequence, with a *PGK-neo* cassette (Fig. 1A). After transfection of the targeting vector into 129/Sv embryonic stem cells by electroporation, two clones of recombination-positive embryonic stem cells were selected by Southern blot analysis using probes at the 5′ and 3′ flanking regions of *Mamld1* and injected into blastocysts. The blastocysts were then transferred into pseudopregnant ICR female mice, to generate chimeric male mice. The chimeric male mice were mated with C57BL/6 female mice, and germline transmission of the mutant gene was confirmed by Southern blot analysis. Subsequently, *Mamld1* KO male mice were produced by mating heterozygous (+/−) female mice with WT male mice. The *Mamld1* KO mouse strain was backcrossed with the C57BL/6 strain and maintained for multiple generations by cross-mating between heterozygous (+/−) female mice and WT male mice.

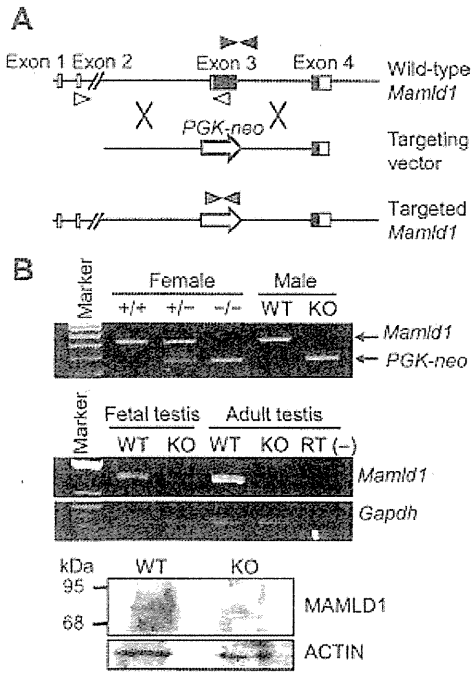

FIG. 1. Generation of *Mamld1* KO mice. A, Schematic representation of the gene targeting procedure. Exon 3 of WT *Mamld1* was replaced by the *PGK-neo* cassette (*PGK-neo*) through homologous recombination indicated by *cross symbols*. The *black and white boxes* denote the coding regions and the untranslated regions, respectively. *Paired black, white, and gray arrowheads* indicate the primer set for amplification of WT *Mamld1* genomic sequence, that for amplification of *Mamld1* transcripts, and that for amplification of Neomycin-resistant gene. B, Confirmation of *Mamld1* KO. Genotyping analysis (*upper panel*), RT-PCR analysis (*middle panel*), and Western blot analysis (*lower panel*) are consistent with successful *Mamld1* KO. +/+, WT female mice; +/−, heterozygous female mice; −/−, homozygous female mice; RT (−), negative control without reverse transcriptase.

In this study, KO male mice of the ninth generation were examined. The noon of the day when a vaginal plug was observed was designated 0.5 d postcoitum (dpc). PCR-based genotyping analysis with tail tissue genomic DNA was performed for *Mamld1*, *PGK-neo*, and *Sry*, using primers shown in Supplemental Table 1, published on The Endocrine Society's Journals Online web site at http://endo.endojournals.org. Body weight and testis weight were measured at birth.

Genital and testicular sample preparation

In the male mice, androgen synthesis starts after approximately 13.5 dpc (10, 11), and morphological characteristics of the male external genitalia are established around 16.5 dpc (12, 13). Thus, genital and testicular samples were prepared from genotype- and embryonic day-matched KO male mice and their WT littermates in the latter half of the fetal life and at birth.

Real-time RT-PCR analyses

Testes from three mice were pooled in a single tube, and five tubes were prepared for each embryonic day. Total RNA was extracted from homogenized samples using ISOGEN (Nippon-gene, Tokyo, Japan), and cDNA was synthesized from 200 ng of total RNA using High Capacity cDNA Reverse Transcription kit (Life Technologies, Carlsbad, CA). Real-time RT-PCR was per-

formed for *Mamld1* and 17 genes involved in sex development and expressed in the fetal testis (*Amh*, *Ar*, *Arx*, *Cyp11a1*, *Cyp17a1*, *Ddx4*, *Dhh*, *Dlx5*, *Dlx6*, *Gata4*, *Hsd17b3*, *Hsd3b1*, *Insl3*, *Nr5a1*, *Ptch1*, *Sox9*, and *Star*) as well as *Gapdh* used as an internal control, using the ABI 7500 Fast real-time PCR system (Life Technologies) and TaqMan gene expression assay kit. Primers and probes used are shown in Supplemental Table 2.

Western blot analysis

Testes collected as described above were homogenized, diluted in Laemmli buffer, and heated at 95 C. Protein extracts were subjected to a standard SDS-PAGE (12% gel) and were hybridized with anti-MAMLD1-antibody (Ab), anti-cytochrome P450 17A1(CYP17A1)-Ab, and anti-3β-hydroxysteroid dehydrogenase (HSD3B)-Ab, as well as anti-ACTIN-Ab (A2066; Sigma, St. Louis, MO) used as an internal control. Anti-MAMLD1-Ab was generated against mouse MAMLD1 peptide (CGSESFLPGSSFAHE) using rabbits, anti-CYP17A1-Ab was purchased from Santa Cruz Biotechnology, Inc. (sc-46081; Santa Cruz, CA), and anti-HSD3B-Ab was as reported previously (14). Chemiluminescence signals were detected using ECL Plus Western Blot Detection kit (GE Healthcare UK Ltd., Buckinghamshire, UK), and signal densities were assessed using an Odyssey Infrared Imaging System (LI-COR Biosciences, Lincoln, NE).

Stereoscopic observation

Morphological findings of external and internal genital regions were examined, as were anogenital distance (AGD) (the distance between the anus and the penoscrotal junction) and AGD index (AGI) (AGD divided by body weight) as indicators for the androgen action during the embryonic period (15–17). Furthermore, whole mount *in situ* hybridization was performed for *sonic hedgehog* (*Shh*), one of the key molecules for the development of genital tubercle (18, 19), using an antisense cRNA fragment as a probe (GenBank accession no. BC063087; nucleotide position, 138-1499). Sense cRNA was used as a negative control. Hybridization was performed using the Wilkinson procedure (20), and signals were visualized with the BM Purple AP Substrate (Roche, Mannheim, Germany).

Histological and immunohistochemical examinations

Histological examination was performed for tissue samples that were fixed with 4% paraformaldehyde, dehydrated, and embedded in paraffin. Serial 6-μm sections were mounted on Superfrost slides, and every tenth section was stained with hematoxylin-eosin.

Immunohistochemical examination was carried out for the remaining section slides that were deparaffinized and incubated with 3% H_2O_2 in PBS to inactivate endogenous peroxidases. The slides were then incubated in blocking solution (Roche) and transferred into a new solution containing polyclonal primary Abs against anti-Mülerian hormone (sc-46081; Santa Cruz Biotechnology, Inc.) as a marker for Sertoli cells, HSD3B as a marker for Leydig cells, DEAD (Asp-Glu-Ala-Asp) box polypeptide 4 (ab13840; Abcam, Cambridge, UK) as a marker for germ cells, and proliferating cell nuclear antigen (PC10; Dako, Glostrup, Denmark) as a marker for proliferating cells. The samples were washed and incubated with secondary Abs conjugated with horseradish peroxidase (Santa Cruz Biotechnology, Inc.). The Simple Stain DAB Solution (Nichirei, Tokyo, Japan) was used for color development. Apoptotic cells were detected by terminal deoxynucleotidyl transferase 2′-deoxyuridine, 5′-triphosphate nick end labeling staining using an *In Situ* Apoptosis Detection kit (TaKaRa Bio, Shiga, Japan). Furthermore, HSD3B-positive cells in four randomly selected fields of each testis were counted, to estimate the number of Leydig cells.

Measurement of intratesticular T and steroid metabolites

Intratesticular T and steroid metabolites were measured at 18.5 dpc by liquid chromatography tandem mass spectrometry (ASKA Pharma Medical, Kanagawa, Japan) using samples stored at −80 C, because intratesticular T usually peaks at 18.5 dpc in normal mice (10, 11).

Cross-mating experiments

Cross-mating was performed between *Mamld1* KO male mice and WT or heterozygous (+/−) female mice and between WT male mice and WT or heterozygous (+/−) female mice.

Statistical analysis

The data are expressed as the mean ± SEM. Statistical significance of the mean between two groups was examined by Student's *t* test, and that of the frequency between two groups was examined by χ^2 test. $P < 0.05$ was considered significant.

Results

Mamld1 expression in the fetal testis of WT male mice

Real-time RT-PCR analyses indicated a gradual and steady increase in the *Mamld1* mRNA levels from 12.5 to 18.5 dpc (Fig. 2).

Generation of *Mamld1* KO male mice

Mamld1 KO male mouse was successfully produced. *Mamld1* exon 3 was deleted from the genome of the KO

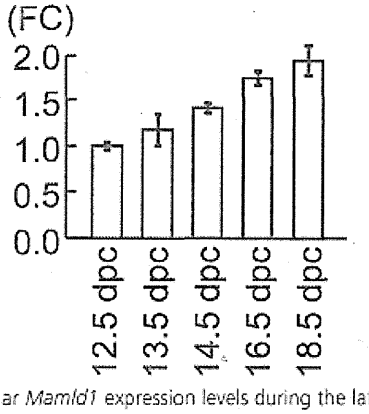

FIG. 2. Testicular *Mamld1* expression levels during the latter half of the fetal life in WT male mice. Figure indicates the data obtained by real-time RT-PCR analyses. Fold change (FC) represents relative mRNA levels of *Mamld1* against *Gapdh*. The relative expression level of *Mamld1* mRNA at 12.5 dpc was designated as 1.0.

TABLE 1. Comparison between *Mamld1* KO mice and their WT littermates

	KO	WT	*P* value
Body weight (g) (at birth)	1.48 ± 0.03 (n = 10)	1.44 ± 0.03 (n = 10)	0.40
AGD (mm) (at birth)	1.33 ± 0.02 (n = 10)	1.32 ± 0.02 (n = 10)	0.62
AGI (mm/g) (at birth)	0.90 ± 0.02 (n = 10)	0.92 ± 0.02 (n = 10)	0.55
Leydig cells (HSD3B-stained cells) (number/HPF) (at 14.5 dpc)	69.3 ± 8.2 (n = 3)	75.1 ± 7.6 (n = 3)	0.63
Testis weight (mg) (at birth)	1.46 ± 0.08 (n = 10)	1.35 ± 0.08 (n = 10)	0.34
Intratesticular steroid metabolites (at 18.5 dpc)			
Pregnenolone (pg/two testes)	17.9 ± 4.0 (n = 4)	15.4 ± 1.4 (n = 4)	0.57
Progesterone (pg/two testes)	16.5 ± 4.6 (n = 4)	15.0 ± 1.7 (n = 4)	0.56
17-OH pregnenolone (pg/two testes)	15.2 ± 2.9 (n = 4)	15.4 ± 1.3 (n = 4)	0.77
17-OH progesterone (pg/two testes)	10.4 ± 1.7 (n = 4)	13.5 ± 2.5 (n = 4)	0.15
Androstenedione (ng/two testes)	0.44 ± 0.15 (n = 4)	0.51 ± 0.07 (n = 4)	0.25
T (ng/two testes)	2.31 ± 0.30 (n = 4)	2.38 ± 0.31 (n = 4)	0.89

Expressed as mean ± SEM. HPF, High power field (234.1 × 175.5 μm).

mice, and neither *Mamld1* mRNA nor MAMLD1 protein was identified in the testis of the KO mice (Fig. 1B). Body weight was comparable between the KO male mice and their WT littermates (Table 1).

Gene and protein expression pattern in the fetal testes of *Mamld1* KO mice

The results are shown in Fig. 3. Relative mRNA levels of *Cyp17a1*, *Hsd3b1*, and *Insl3* mRNAs were mildly but

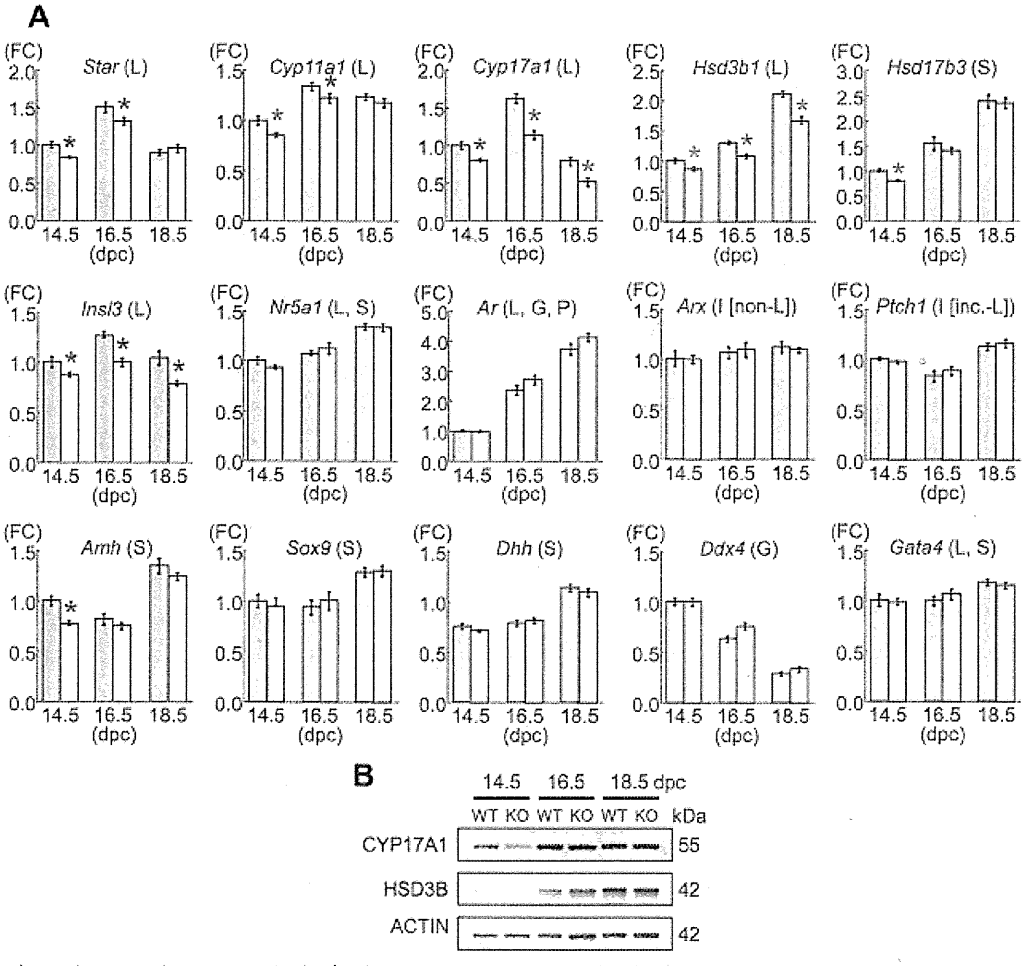

FIG. 3. Gene and protein expression patterns in the fetal testes. A, Relative mRNA levels of examined genes against *Gapdh*. FC, Fold change; L, Leydig cells; S, Sertoli cells; G, germ cells; P, peritubular cells; I [non-L], interstitial cells excluding Leydig cells; I [inc.-L], interstitial cells including Leydig cells. The *green and the yellow bars* indicate the data obtained from WT male mice and *Mamld1* KO male, respectively. For each gene, the relative expression level of mRNA in WT male mice at 14.5 dpc was designated as 1.0. *Red asterisks* indicate significant results ($P < 0.05$). B, Western blot analysis for CYP17A1 and HSD3B, as well as for ACTIN.

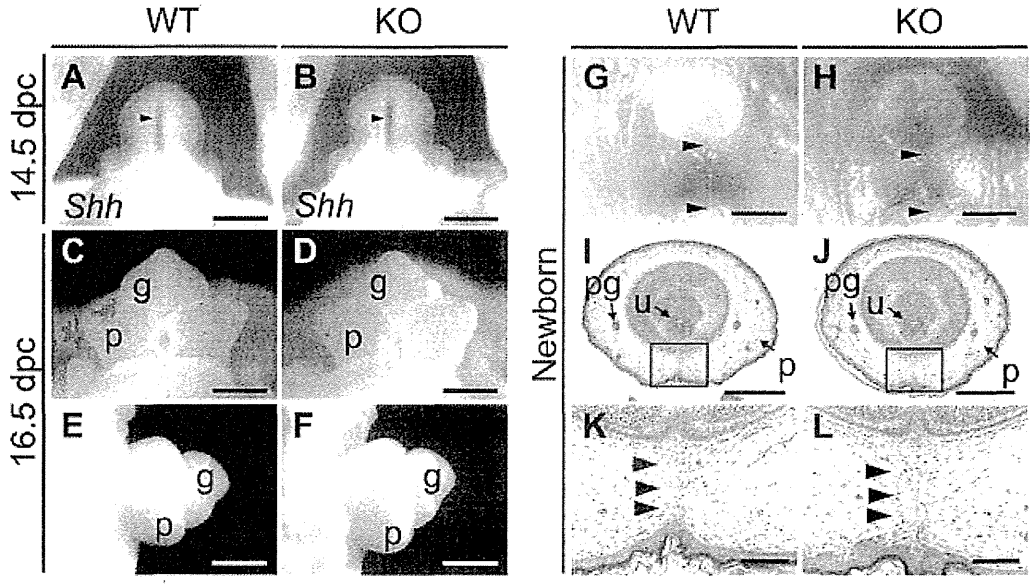

FIG. 4. External genitalia of WT and *Mamld1* KO male mice. A and B, Whole mount *in situ* hybridization for *Shh* (*arrowheads*) in the developing genital region at 14.5 dpc. C–F, Appearance of the genital tubercle at 16.5 dpc. G and H, Appearance of the external genitalia at birth. The distance between the anus and the penoscrotal junction (*arrowheads*) represents the AGD. I–L, Histological findings of the external genitalia at birth. *Arrowheads* in K and L indicate the fused prepuce. g, Glans; p, prepuce; pg, preputal gland; u, urethra. *Scale bars*: 500 μm (A–F, I, and J), 1 mm (G and H), and 100 μm (K and L).

significantly lower in the KO male mice than in their WT littermates at 14.5, 16.5, and 18.5 dpc, as were those for *Star* and *Cyp11a1* at 14.5 and 16.5 dpc (65–80%) (*Dlx5* and *Dlx6* expression levels were extremely low). By contrast, relative mRNA levels of the remaining genes were comparable between the KO male mice and their WT littermates, except for relative mRNA levels of *Hsd17b3* and *Amh* at 14.5 dpc. However, expression levels of CYP17A1 and HSD3B proteins were similar between the KO male mice and their WT littermates and were obviously higher at 16.5 and 18.5 dpc than at 14.5 dpc.

External genital findings of *Mamld1* KO male mice

External genitalia were obviously normal in the *Mamld1* KO male mice (Fig. 4 and Table 1). *Shh* was normally expressed in the urethral epithelium of the KO male mice at 14.5 dpc, and subsequent outgrowth of genital tubercle and fusion of the urethral folds at the ventral midline occurred in the KO male mice at the same embryonic stages as in their WT littermates. Furthermore, external genitalia were normally developed at birth, with the comparable AGD and AGI between the KO mice and their WT littermates.

Internal genital findings of *Mamld1* KO mice

Internal genitalia of the *Mamld1* KO male mice were also free from demonstrable abnormality (Fig. 5 and Table 1). Intraabdominal testicular descent, wolffian development, and müllerian regression were normally observed in the KO male mice at 16.5 dpc. Testicular histological findings were comparable between the KO mice and their WT littermates at 14.5 dpc and at birth. Immunohistochemical findings indicated the presence of similar numbers of Sertoli cells (anti-Müllerian hormone-stained cells), Leydig cells (HSD3B-stained cells), and germ cells [DEAD (Asp-Glu-Ala-Asp) box polyoeotide 4-stained cells] at 14.5 dpc as well as the presence of a similar number of Leydig cells (HSD3B-stained cells) at birth between the KO mice and their WT littermates. A relatively large number of mitotic cells (proliferating cell nuclear antigen-stained cells) was also identified in both the KO mice and their WT littermates, as were a small number of apoptotic cells (terminal deoxynucleotidyl transferase 2′-deoxyuridine, 5′-triphosphate nick end labeling-stained cells) (data not shown). In addition, testis weights at birth and intratesticular concentrations of T and other steroid metabolites at 18.5 dpc were also similar between the KO mice and their WT littermates.

Cross-mating experiments

The results are shown in Table 2. *Mamld1* KO male mice produced offspring with WT and heterozygous (+/−) female mice, as did WT male mice. Furthermore, the frequency of littermate offspring [*Mamld1* KO male mice, WT male mice, homozygous (−/−) female mice, heterozygous (+/−) female mice, and WT female mice] was in agreement with the expected Mendelian mode of inheritance.

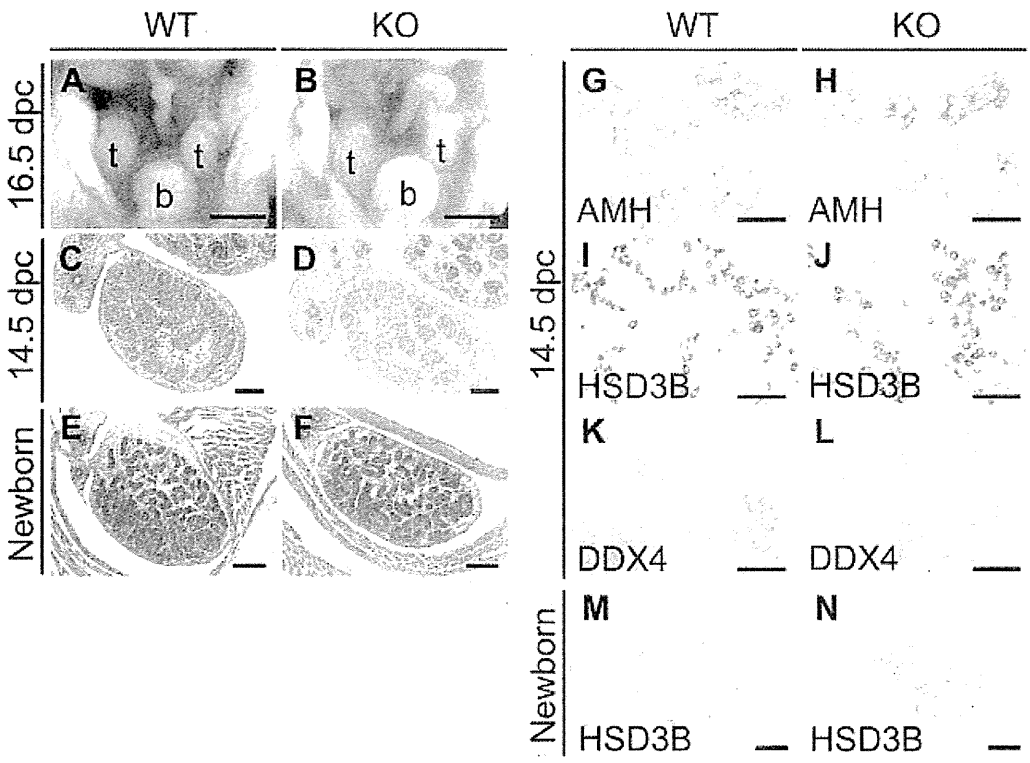

FIG. 5. Internal genitalia of WT and *Mamld1* KO male mice. A and B, Appearance of internal genital organs at 16.5 dpc. C–F, Histological findings of testes at 14.5 dpc and birth. G–N, Immunohistochemical findings of testes at 14.5 dpc and birth. b, Bladder; t, testis. *Scale bars*: 1 mm (A and B), 100 μm (C and D), 200 μm (E, F, M, and N), and 50 μm (G–L).

Discussion

The *Mamld1* mRNA expression was gradually and steadily increased from 12.5 to 18.5 dpc in the fetal testis of WT male mice. In this regard, intratesticular T has also been reported to increase in a similar manner in the mouse (10, 11). In addition, human study has also revealed clear *MAMLD1* expression in the fetal testis. These findings would argue for a positive role of *MAMLD1/Mamld1* in the T production in the fetal testis (1, 21).

We generated and studied *Mamld1* KO male mice. The results are summarized as follows: 1) mRNA levels of genes exclusively expressed in Leydig cells (*Star*, *Cyp11a1*, *Cyp17a1*, *Hsd3b1*, and *Insl3*) were mildly but significantly reduced, whereas those of genes expressed in other cell types or in Leydig and other cell types grossly remained normal (*Hsd17b3* is expressed in Sertoli cells of the fetal testis, although it is expressed in Leydig cells of the adult testis) (22, 23); 2) despite such mild reduction of mRNA levels, CYP17A1 and HSD3B proteins were sufficiently produced; 3) no demonstrable abnormality was identified by detailed studies for the external and internal genital regions; and 4) the *Mamld1* KO male mice retained normal fertility. Collectively, these findings imply that *Mamld1* deficiency reduces mRNA expression levels of multiple, if not all, genes expressed in mouse fetal Leydig cells but permits normal genital development and reproductive function. In support of this notion, such discrepancy between mRNA levels and protein levels as well as phenotypic consequences has been reported previously (24–26). Indeed, Greenbaum *et al.* (27) have proposed three possible explanations for the poor correlations between mRNA and protein expression levels: 1) there are many complicated and varied posttranscriptional mechanisms involved in turning mRNA into protein that are not yet sufficiently well defined; 2) proteins may differ substantially in their *in vivo* half lives; and 3) there may be a significant amount of error and noise in both protein and mRNA experiments that limit our ability to get a clear picture. These explanations would also apply to our results indicating normal expression of CYP17A1 and HSD3B proteins, in the presence of mildly but significantly reduced expression of *Cyp17a1* and *Hsd3b1* mRNAs. Furthermore, because CYP17A1 and HSD3B protein levels increased in a manner grossly similar to that reported for intratesticular T (10, 11) in both the *Mamld1* KO male mice and their WT littermates, this would be consistent with the apparently normal testicular function of the *Mamld1* KO male mice.

The normal phenotype in the *Mamld1* KO male mice is contrastive to the DSD phenotype in the *MAMLD1* mu-

TABLE 2. Cross-mating experiments for *Mamld1*

Offspring produced by cross-mating between *Mamld1* KO male mice (n = 5) and WT female mice (n = 24)					
Sex and *Mamld1* genotype	Male (−)	Male (+)	Female (−/−)	Female (+/−)	Female (+/+)
Number and frequency	n/o	89 (45.6%)	n/o	106 (54.4%)	n/o
Offspring produced by cross-mating between *Mamld1* KO male mice (n = 14) and heterozygous female mice (n = 49)					
Sex and *Mamld1* genotype	Male (−)	Male (+)	Female (−/−)	Female (+/−)	Female (+/+)
Number and frequency	84 (23.6%)	96 (27.0%)	94 (26.4%)	82 (23.0%)	n/o
Offspring produced by cross-mating between WT male mice (n = 6) and WT female mice (n = 12)					
Sex and *Mamld1* genotype	Male (−)	Male (+)	Female (−/−)	Female (+/−)	Female (+/+)
Number and frequency	n/o	58 (59.8%)	n/o	n/o	39 (40.2%)
Offspring produced by cross-mating between WT male mice (n = 9) and heterozygous female mice (n = 46)					
Sex and *Mamld1* genotype	Male (−)	Male (+)	Female (−/−)	Female (+/−)	Female (+/+)
Number and frequency	86 (25.3%)	85 (25.0%)	n/o	84 (24.7%)	85 (25.0%)

WT or +, WT; KO or −, *Mamld1* KO; n/o, not obtained.

tation positive patients (1, 3). In this regard, it is notable that male genital development is primarily induced by testicular T that is produced via Δ^5-pathway under the stimulation of chorionic gonadotropin during the first trimester in the human (28–31), whereas it is primarily carried out by testicular T that is produced via Δ^4-pathway independently of the chorionic gonadotropin stimulation during the late gestational period in the mouse (10, 31, 32). Thus, although the detailed mechanism(s) remains to be clarified, such species difference in the fetal male sex development may underlie the phenotypic difference between the *Mamld1* KO male mice and the *MAMLD1* mutation positive patients. In addition, the bias that individuals with abnormal phenotypes only are usually examined in the human study may also be relevant to this matter.

The results of mRNA expression levels and intratesticular hormone concentrations in the *Mamld1* KO male mice are different from those identified by transient *Mamld1* knockdown experiments using siRNAs and MLTCs (6, 8), although the normal Leydig cell number of the *Mamld1* KO male mice appears to be consistent with the sustained proliferation of siRNA-transfected MLTCs (8). Indeed, *Mamld1* knockdown has predominantly affected *Cyp17a1* expression (8) and significantly decreased T and other steroid metabolite after 17α-hydroxylation (6, 8). However, MLTCs are derived from adult Leydig tumor cells and are characterized by a markedly low 17α-hydroxylase activity and a well-preserved 17/20 lyase activity for both Δ^4- and Δ^5-pathways (33). Such unique properties of MLTCs may be relevant to the preferential impairment of *Cyp17a1* expression and 17α-hydroxylation in siRNA-transfected MLTCs.

Two findings also appear to be worth pointing out in this study. First, *Insl3* mRNA expression was significantly reduced and *Amh* mRNA expression was grossly normal, in the *Mamld1* KO mice. Such mRNA expression patterns, if they also take place in the human, would be relevant to the frequent occurrence of cryptorchidism and the lack of müllerian derivatives in patients with *MAMLD1* mutations (1). Second, *Mamld1* KO male mice, WT male mice, homozygous (−/−) female mice, heterozygous (+/−) female mice, and WT female mice were born with frequencies consistent with the Mendelian mode of inheritance. Thus, although *Mamld1* is ubiquitously expressed with strong expressions in the central nervous system (1), *Mamld1* deficiency is unlikely to affect viability.

In summary, the present study implies that *Mamld1* enhances mRNA expression levels of multiple genes exclusively expressed in fetal Leydig cells, although the effects of *Mamld1* deficiency are insufficient to compromise the genital and reproductive development. Further studies will permit a better clarification of the biological function of *MAMLD1/Mamld1*.

Acknowledgments

Address all correspondence and requests for reprints to: Professor Tsutomu Ogata, Department of Pediatrics, Hamamatsu University School of Medicine, Hamamatsu 431-3192, Japan. E-mail: tomogata@hama-med.ac.jp.

This work was supported by the National Center for Child Health and Development Grant 23A-1; Grant for Research on Intractable Diseases from the Ministry of Health, Labor, and

Welfare; Environment Research and Technology Development Fund C-0905 of the Ministry of Environment; Grants-in-Aid for Scientific Research (B) 23390249 and (S) 22227002 and for Young Scientists (B) 24790303 from the Japan Society for the Promotion of Science; and Grant-in-Aid for Scientific Research on Innovative Areas 22132004 from the Ministry of Education, Culture, Sports, Science, and Technology.

Disclosure Summary: The authors have nothing to disclose.

References

1. **Fukami M, Wada Y, Miyabayashi K, Nishino I, Hasegawa T, Nordenskjöld A, Camerino G, Kretz C, Buj-Bello A, Laporte J, Yamada G, Morohashi K, Ogata T** 2006 CXorf6 is a causative gene for hypospadias. Nat Genet 38:1369–1371
2. **Kalfa N, Liu B, Klein O, Ophir K, Audran F, Wang MH, Mei C, Sultan C, Baskin LS** 2008 Mutations of CXorf6 are associated with a range of severities of hypospadias. Eur J Endocrinol 159:453–458
3. **Ogata T, Laporte J, Fukami M** 2009 MAMLD1 (CXorf6): a new gene involved in hypospadias. Horm Res 71:245–252
4. **Chen Y, Thai HT, Lundin J, Lagerstedt-Robinson K, Zhao S, Markljung E, Nordenskjöld A** 2010 Mutational study of the MAMLD1-gene in hypospadias. Eur J Med Genet 53:122–126
5. **van der Zanden LF, van Rooij IA, Feitz WF, Franke B, Knoers NV, Roeleveld N** 2012 Aetiology of hypospadias: a systematic review of genes and environment. Hum Reprod Update 18:260–283
6. **Fukami M, Wada Y, Okada M, Kato F, Katsumata N, Baba T, Morohashi K, Laporte J, Kitagawa M, Ogata T** 2008 Mastermind-like domain-containing 1 (MAMLD1 or CXorf6) transactivates the Hes3 promoter, augments testosterone production, and contains the SF1 target sequence. J Biol Chem 283:5525–5532
7. **Lin L, Achermann JC** 2008 Steroidogenic factor-1 (SF-1, Ad4BP, NR5A1) and disorders of testis development. Sex Dev 2:200–209
8. **Nakamura M, Fukami M, Sugawa F, Miyado M, Nonomura K, Ogata T** 2011 Mamld1 knockdown reduces testosterone production and Cyp17a1 expression in mouse Leydig tumor cells. PLoS One 6:e19123
9. **Hogan B, Beddington R, Costantini F, Lacy E** 1994 Manipulating the mouse embryo: a laboratory manual. New York: Cold Spring Harbor Laboratory Press
10. **O'Shaughnessy PJ, Baker P, Sohnius U, Haavisto AM, Charlton HM, Huhtaniemi I** 1998 Fetal development of Leydig cell activity in the mouse is independent of pituitary gonadotroph function. Endocrinology 139:1141–1146
11. **O'Shaughnessy PJ, Baker PJ, Johnston H** 2006 The foetal Leydig cell-differentiation, function and regulation. Int J Androl 29:90–95; discussion 105–108
12. **Miyagawa S, Satoh Y, Haraguchi R, Suzuki K, Iguchi T, Taketo MM, Nakagata N, Matsumoto T, Takeyama K, Kato S, Yamada G** 2009 Genetic interactions of the androgen and Wnt/β-catenin pathways for the masculinization of external genitalia. Mol Endocrinol 23:871–880
13. **Suzuki K, Ogino Y, Murakami R, Satoh Y, Bachiller D, Yamada G** 2002 Embryonic development of mouse external genitalia: insights into a unique mode of organogenesis. Evol Dev 4:133–141
14. **Fatchiyah, Zubair M, Shima Y, Oka S, Ishihara S, Fukui-Katoh Y, Morohashi K** 2006 Differential gene dosage effects of Ad4BP/SF-1 on target tissue development. Biochem Biophys Res Commun 341:1036–1045
15. **Graham S, Gandelman R** 1986 The expression of ano-genital distance data in the mouse. Physiol Behav 36:103–104
16. **Kerin TK, Vogler GP, Blizard DA, Stout JT, McClearn GE, Vandenbergh DJ** 2003 Anogenital distance measured at weaning is correlated with measures of blood chemistry and behaviors in 450-day-old female mice. Physiol Behav 78:697–702
17. **Swan SH, Main KM, Liu F, Stewart SL, Kruse RL, Calafat AM, Mao CS, Redmon JB, Ternand CL, Sullivan S, Teague JL** 2005 Decrease in anogenital distance among male infants with prenatal phthalate exposure. Environ Health Perspect 113:1056–1061
18. **Haraguchi R, Mo R, Hui C, Motoyama J, Makino S, Shiroishi T, Gaffield W, Yamada G** 2001 Unique functions of Sonic hedgehog signaling during external genitalia development. Development 128:4241–4250
19. **Miyagawa S, Matsumaru D, Murashima A, Omori A, Satoh Y, Haraguchi R, Motoyama J, Iguchi T, Nakagata N, Hui CC, Yamada G** 2011 The role of sonic hedgehog-Gli2 pathway in the masculinization of external genitalia. Endocrinology 152:2894–2903
20. **Wilkinson D** 1992 *In situ* hybridization: a practical approach. London: Oxford University Press
21. **O'Shaughnessy PJ, Baker PJ, Monteiro A, Cassie S, Bhattacharya S, Fowler PA** 2007 Developmental changes in human fetal testicular cell numbers and messenger ribonucleic acid levels during the second trimester. J Clin Endocrinol Metab 92:4792–4801
22. **Baker PJ, Sha JH, O'Shaughnessy PJ** 1997 Localisation and regulation of 17β-hydroxysteroid dehydrogenase type 3 mRNA during development in the mouse testis. Mol Cell Endocrinol 133:127–133
23. **O'Shaughnessy PJ, Baker PJ, Heikkilä M, Vainio S, McMahon AP** 2000 Localization of 17β-hydroxysteroid dehydrogenase/17-ketosteroid reductase isoform expression in the developing mouse testis-androstenedione is the major androgen secreted by fetal/neonatal leydig cells. Endocrinology 141:2631–2637
24. **Lehmann KP, Phillips S, Sar M, Foster PM, Gaido KW** 2004 Dose-dependent alterations in gene expression and testosterone synthesis in the fetal testes of male rats exposed to di (n-butyl) phthalate. Toxicol Sci 81:60–68
25. **Thompson CJ, Ross SM, Hensley J, Liu K, Heinze SC, Young SS, Gaido KW** 2005 Differential steroidogenic gene expression in the fetal adrenal gland versus the testis and rapid and dynamic response of the fetal testis to di(n-butyl) phthalate. Biol Reprod 73:908–917
26. **Weisser J, Landreh L, Söder O, Svechnikov K** 2011 Steroidogenesis and steroidogenic gene expression in postnatal fetal rat Leydig cells. Mol Cell Endocrinol 341:18–24
27. **Greenbaum D, Colangelo C, Williams K, Gerstein M** 2003 Comparing protein abundance and mRNA expression levels on a genomic scale. Genome Biol 4:117
28. **Flück CE, Miller WL, Auchus RJ** 2003 The 17, 20-lyase activity of cytochrome p450c17 from human fetal testis favors the Δ5 steroidogenic pathway. J Clin Endocrinol Metab 88:3762–3766
29. **Fowler PA, Bhattacharya S, Gromoll J, Monteiro A, O'Shaughnessy PJ** 2009 Maternal smoking and developmental changes in luteinizing hormone (LH) and the LH receptor in the fetal testis. J Clin Endocrinol Metab 94:4688–4695
30. **Huhtaniemi IT, Korenbrot CC, Jaffe RB** 1977 HCG binding and stimulation of testosterone biosynthesis in the human fetal testis. J Clin Endocrinol Metab 44:963–967
31. **Scott HM, Mason JI, Sharpe RM** 2009 Steroidogenesis in the fetal testis and its susceptibility to disruption by exogenous compounds. Endocr Rev 30:883–925
32. **Baker PJ, O'Shaughnessy PJ** 2001 Role of gonadotrophins in regulating numbers of Leydig and Sertoli cells during fetal and postnatal development in mice. Reproduction 122:227–234
33. **Panesar NS, Chan KW, Ho CS** 2003 Mouse Leydig tumor cells produce C-19 steroids, including testosterone. Steroids 68:245–251

Hindawi Publishing Corporation
International Journal of Endocrinology
Volume 2012, Article ID 584807, 8 pages
doi:10.1155/2012/584807

Review Article

Molecular Bases and Phenotypic Determinants of Aromatase Excess Syndrome

Maki Fukami,[1] Makio Shozu,[2] and Tsutomu Ogata[1,3]

[1] *Department of Molecular Endocrinology, National Research Institute for Child Health and Development, 2-10-1 Ohkura, Setagaya, Tokyo 157-8535, Japan*
[2] *Department of Reproductive Medicine, Graduate School of Medicine, Chiba University, 1-8-1 Inohana, Chuo-ku, Chiba City 206-8670, Japan*
[3] *Department of Pediatrics, Hamamatsu University School of Medicine, 1-20-1 Handayama, Higashi-ku, Shizuoka, Hamamatsu 431-3192, Japan*

Correspondence should be addressed to Maki Fukami, mfukami@nch.go.jp

Received 9 July 2011; Revised 22 September 2011; Accepted 2 October 2011

Academic Editor: Rodolfo Rey

Copyright © 2012 Maki Fukami et al. This is an open access article distributed under the Creative Commons Attribution License, which permits unrestricted use, distribution, and reproduction in any medium, provided the original work is properly cited.

Aromatase excess syndrome (AEXS) is a rare autosomal dominant disorder characterized by gynecomastia. This condition is caused by overexpression of *CYP19A1* encoding aromatase, and three types of cryptic genomic rearrangement around *CYP19A1*, that is, duplications, deletions, and inversions, have been identified in AEXS. Duplications appear to have caused *CYP19A1* overexpression because of an increased number of physiological promoters, whereas deletions and inversions would have induced wide *CYP19A1* expression due to the formation of chimeric genes consisting of a noncoding exon(s) of a neighboring gene and *CYP19A1* coding exons. Genotype-phenotype analysis implies that phenotypic severity of AEXS is primarily determined by the expression pattern of *CYP19A1* and the chimeric genes and by the structural property of the fused exons with a promoter function (i.e., the presence or the absence of a natural translation start codon). These results provide novel information about molecular mechanisms of human genetic disorders and biological function of estrogens.

1. Introduction

Aromatase encoded by *CYP19A1* is a cytochrome P450 enzyme that plays a key role in estrogen biosynthesis [1]. It catalyzes the conversion of Δ^4-androstendione into estrone (E_1) and that of testosterone (T) into estradiol (E_2) in the placenta and ovary as well as in other tissues such as the fat, skin, bone, and brain [1].

Overexpression of *CYP19A1* causes a rare autosomal dominant disorder referred to as aromatase excess syndrome (AEXS, OMIM no. 139300) [2–8]. AEXS is characterized by pre- or peripubertal onset gynecomastia, gonadal dysfunction, advanced bone age from childhood to pubertal period, and short adult height in affected males [2–8]. In particular, gynecomastia is a salient feature in AEXS, and, therefore, this condition is also known as hereditary gynecomastia or familial gynecomastia [5]. Affected females may also show several clinical features such as macromastia, precocious puberty, irregular menses, and short adult height [5, 6, 8].

Recently, three types of cryptic genomic rearrangements around *CYP19A1* have been identified in 23 male patients with AEXS [2–4]. The results provide useful implications not only for the clarification of underlying mechanisms but also for the identification of phenotypic determinants. Here, we review the current knowledge about AEXS.

2. The Aromatase Gene (*CYP19A1*)

CYP19A1 encoding aromatase is located on 15q21.2 adjacent to *DMXL2* and *GLDN* (Figure 1) [3, 9]. It spans ~123 kb and consists of at least 11 noncoding exons 1 and nine coding exons 2–10 [9–12]. Each exon 1 is accompanied by a tissue-specific promoter and is spliced alternatively onto a common splice acceptor site at exon 2, although some transcripts are known to contain two of the exons 1 probably due to a splice error [9–11]. Transcription of *CYP19A1* appears to be tightly regulated by alternative usage of the multiple

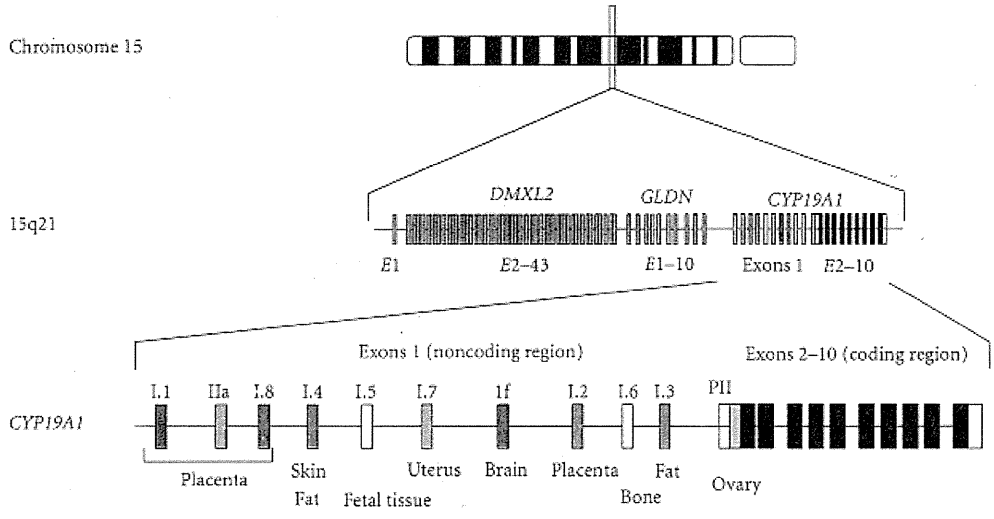

FIGURE 1: Simplified schematic representation indicating the genomic structure of *CYP19A1*. *CYP19A1* is located on 15q21.2 adjacent to *DMXL2* and *GLDN* and consists of at least 11 noncoding exons 1 and nine coding exons 2–10 [9, 10]. Each exon 1 is accompanied by a tissue-specific promoter and is spliced alternatively onto a common splice acceptor site at exon 2 [9–13].

promoters [9–13]. Actually, *CYP19A1* is strongly expressed in the placenta and moderately expressed in the ovary, whereas it is only weakly expressed in a rather limited number of tissues including skin, fat, and hypothalamus [4, 13]. Of the 11 noncoding exons 1, exon I.4 seems to play a critical role in the regulation of estrogen biosynthesis in males, because this exon contains the major promoter for extragonadal tissues [9, 10].

3. Molecular Bases of AEXS

A family with dominantly transmitted gynecomastia of prepubertal onset was first described in 1962 by Wallach and Garcia [14]. After this initial report, several cases have been described [5–8, 15]. Laboratory examinations of the affected males revealed markedly elevated serum estrogen values and estrogen/androgen ratios and significantly increased aromatase activity in fibroblasts and lymphocytes [5–8, 15]. Linkage analyses in two families indicated a close association between *CYP19A1*-flanking polymorphic markers and the disease phenotype [5, 6]. Thus, the condition was assumed to be caused by gain-of-function mutations of *CYP19A1*, and, therefore, the name of AEXS was coined for this condition [7, 8]. However, since direct sequencing and Southern blotting analysis failed to detect mutations or copy number abnormalities in the coding region of *CYP19A1* [5, 6], the molecular basis of this entity remained elusive until recently.

In 2003, Shozu et al. reported a father-son pair and a sporadic case with AEXS in whom they identified heterozygous chromosomal inversions of the chromosome 15 [2]. Subsequently, Demura et al. performed detailed molecular studies for these cases and additional two cases and characterized four types of inversions affecting the 5′ region of *CYP19A1* [3]. Each inversion has resulted in the formation of a chimeric gene consisting of *CYP19A1* coding exons and exon 1 of the widely expressed neighboring genes, that is, *CGNL1*, *TMOD3*, *MAPK6*, and *TLN2*. These data imply that overexpression of *CYP19A1* in the inversion-positive cases are caused by cryptic usage of constitutively active promoters. Consistent with this, *in silico* analysis revealed the presence of promoter-compatible sequences around exon 1 of *CGN1*, *TMOD3*, and *MAPK6* in multiple cell types, although such sequences remain to be identified for noncoding exons of *TLN2* [4].

We recently studied 18 males from six families with AEXS (families A–F) and identified three types of heterozygous cryptic genomic rearrangements in the upstream region of the *CYP19A1* coding exons (Figure 2) [4]. In families A and B, we identified the same 79,156 bp tandem duplication encompassing seven of the 11 noncoding exons 1 of *CYP19A1*. Notably, this duplication includes exon I.4 that functions as a major promoter for extragonadal tissues such as fat and skin; therefore, *CYP19A1* overexpression in these families would be explained by increasing the number of this promoter. Indeed, RT-PCR analysis detected a splice variant consisting of exon I.4 at the 5′ side and exon I.8 at the 3′ side in lymphoblastoid cell lines and skin fibroblasts of the patients, indicating that the duplicated exon I.4 at the distal nonphysiological position actually functions as transcription start sites. In family C, we identified a 211,631 bp deletion affecting exons 2–43 of *DMXL2* and exons 5–10 of *GLDN*. This deletion appears to have caused *CYP19A1* overexpression because of cryptic usage of *DMXL2* exon 1 as an extra transcription start site for *CYP19A1*. Indeed, RT-PCR revealed the presence of chimeric mRNA clones consisting of *DMXL2* exon 1 and *CYP19A1* exon 2, supporting the notion that aberrant splicing has occurred between these two exons. Such *DMXL2/CYP19A1* chimeric mRNA accounted for 2–5% of *CYP19A1*-containing transcripts from skin fibroblasts. In families D–F, we identified

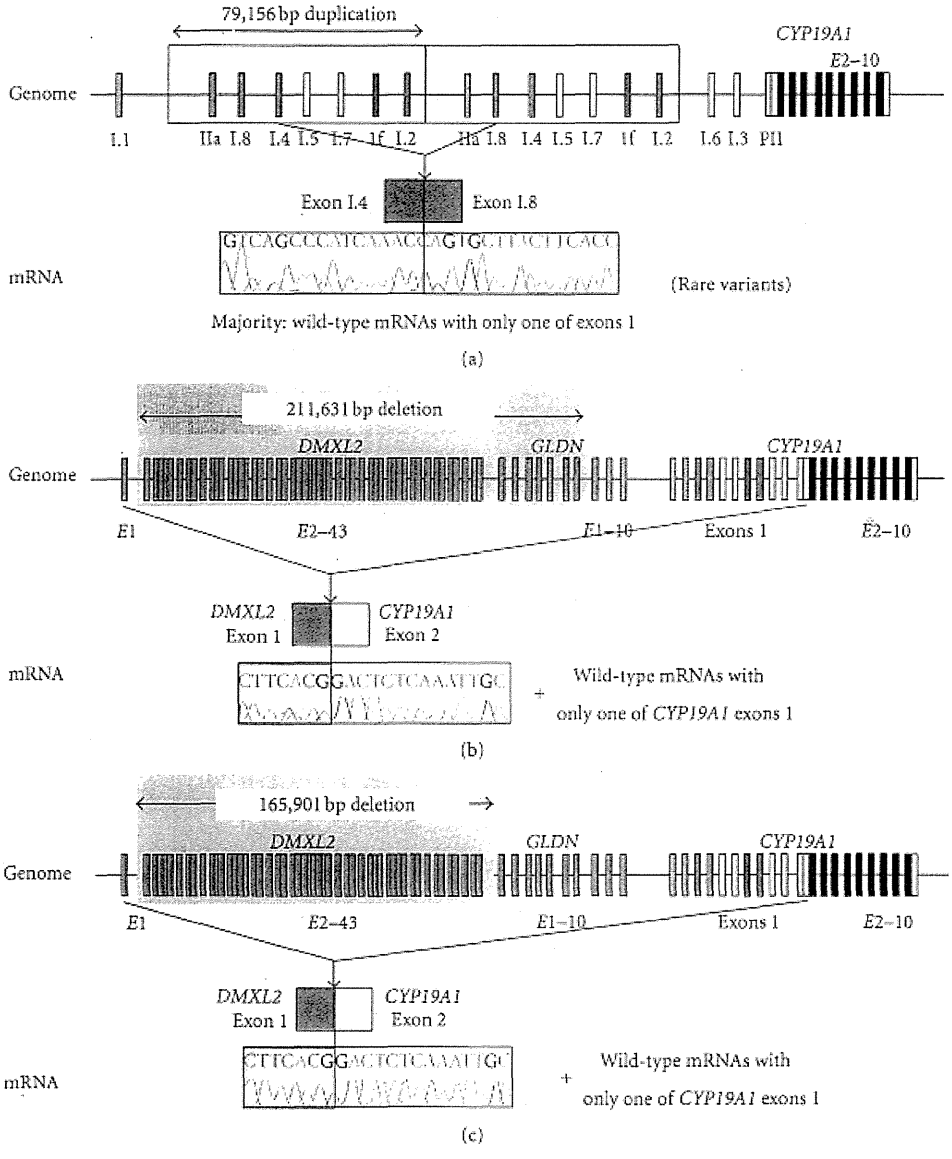

FIGURE 2: Schematic representation of duplications and deletions identified in patients with AEXS. (a) the tandem duplication of families A and B [4]. Genome: the duplication (yellow boxes) includes seven of the 11 noncoding exons 1 of *CYP19A1*. mRNA: the sequence of a rare transcript is shown. The 3′-end of exon I.4 is connected with the 5′-end of exon I.8. (b) The deletion of family C [4]. Genome: the deletion (a gray area) includes exons 2–43 of *DMXL2* and exons 5–10 of *GLDN*. mRNA: The sequence of a rare chimeric gene transcript is shown. *DMXL2* exon 1 consisting of a noncoding region and a coding region is spliced onto the common acceptor site of *CYP19A1* exon 2. (c) The deletion of families D–F [4]. Genome: the deletion (a gray area) includes exons 2–43 of *DMXL2*. mRNA: the sequence of a rare chimeric gene transcript is delineated. The mRNA structure is the same as that detected in family C.

an identical 165,901 bp deletion including exons 2–43 of *DMXL2*. RT-PCR identified the same chimeric mRNA as that detected in family C.

Collectively, three types of genomic rearrangements on 15q21 have been identified in AEXS to date, namely, inversion type (four subtypes), duplication type, and deletion type (two subtypes) (Figure 3(a)) [2–4]. In this regard, sequence analyses for the breakpoints have indicated that (1) inversion types are formed by a repeat sequence-mediated nonallelic intrachromosomal or interchromosomal recombination or by a replication-based mechanism of fork stalling and template switching (FoSTeS) that occurs in the absence of repeat sequences and is often associated with microhomology [16], (2) duplication type is generated by FoSTeS, and (3) deletions are produced by nonhomologous end joining that takes place between nonhomologous sequences and is frequently accompanied by an insertion of a short segment at the fusion point or by a nonallelic recombination [16].

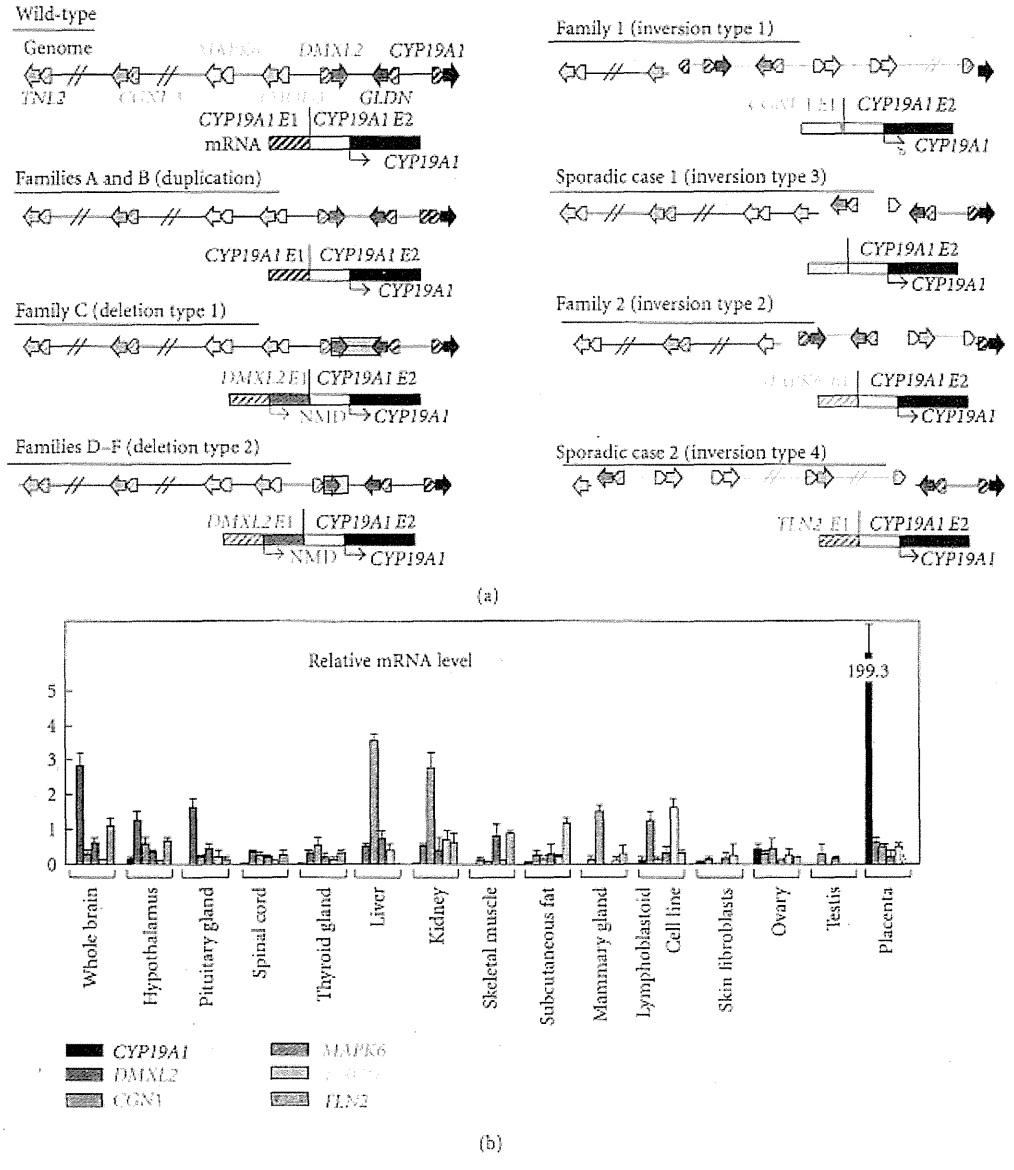

FIGURE 3: Structural and functional properties of the fused exons. (a) Schematic representation of the rearranged genome and mRNA structures. The white and the black boxes of *CYP19A1* exon 2 show untranslated region and coding region, respectively. For genome, the striped and the painted arrows indicate noncoding and coding exons, respectively (5′ → 3′). The inverted genomic regions are delineated in blue lines. For mRNA, colored striped boxes represent noncoding regions of each gene. The *DMXL2-CYP19A1* chimeric mRNA has two translation initiation codons and therefore is destined to produce not only *CYP19A1* protein but also a 47 amino acid protein which is predicted to undergo nonsense-mediated mRNA decay (NMD). The deletion and the inversion types are associated with heterozygous impairment of neighboring genes (deletion or disconnection between noncoding exon(s) and the following coding exons). The inversion subtype 1 is accompanied by inversion of eight of the 11 *CYP19A1* exons 1, and the inversion subtype 2 is associated with inversion of the placenta-specific *CYP19A1* exon I.1. (b) Expression patterns of *CYP19A1* and the five neighboring genes involved in the chimeric gene formation [4]. Relative mRNA levels against *TBP* in normal human tissues are shown.

Thus, it appears that genomic sequence around *CYP19A1* harbors particular motifs that are vulnerable to replication- and recombination-mediated errors. The results provide novel mechanisms of gain-of-function mutations leading to human diseases.

4. Clinical Features of AEXS

To date, a total of 23 male cases from 10 families have been reported to have molecularly confirmed AEXS (Table 1, Figure 3(a)) [2–4]. They exhibited pre- or peripubertal onset

Table 1: Summary of clinical studies in male patients with aromatase excess syndrome (modified from [4]).

(a)

Family			Family A		Family B		Family C			Family D			Family E	
Mutation types			Duplication		Duplication		Deletion			Deletion			Deletion	
The promoter involved in *CYP19A1* overexpression			*CYP19A1*		*CYP19A1*		*CYP19A1*			*DMXL2*			*DMXL2*	
Case		Case 1	Case 2	Case 3	Case 4		Case 5	Case 6	Case 7	Case 8	Case 9		Case 10	
Age at examination (year)		66	15	20	15		15	13	42	9	12		13	
<Phenotypic findings>														
Gynecomastia (tanner breast stage)		2	2	2	3		4	4	4	3	4		4	
Onset of gynecomastia (year)		13	13	10	11		12	11	11	7	9		10	
Mastectomy (year)		No	Yes (15)	No	Yes (15)		Yes (15)	Yes (13)	No	No	Yes (12)		Yes (13)	
Testis (ml)		N.E.	12	12	12		12	12	N.E.	3	12		20	
Pubic hair (tanner stage)		N.E.	2-3	4	5		4	3	N.E.	1	3		4	
Facial hair		Normal	Scarce	Scarce	Normal		Absent	Absent	N.E.	Absent	Absent		Absent	
Height (SDS)[a]		−1.2	−0.3	+0.4	+0.8		−2.0	−1.0	−1.6	+2.7	±0		+1.8	
Bone age (year)[b]		N.E.	N.E.	N.E.	16.0		16.0	13.5	N.E.	13.0	15.0		17.0	
Fertility (spermatogenesis)		Yes	?	(Yes)[h]	?		?	?	Yes	?	?		?	
<Endocrine findings>[c]		B	B	S	B	S	B	S	B	S	B	S	B	B	S	B	S	B	S
<At Dx>	Stimulus																		
LH (mIU/mL)	GnRH[e]	3.8	2.3	14.3	2.1	17.0	2.4	29.4	1.9	40.6	1.8	69.2		1.1	11.5	0.6	39.5	6.7	14.8
LH (mIU/mL)	GnRH (after priming)[f]		1.8	9.5	1.3	10.7													
FSH (mIU/mL)	GnRH[e]	1.7	3.1	5.3	<0.5	1.2	0.9	2.4	1.4	4.2	2.0	7.8		3.2	6.6	0.6	2.9	0.7	1.0
FSH (mIU/mL)	GnRH (after priming)[f]		2.6	3.2	<0.5	0.9													
Prolactin (ng/ml)			4.3		5.3				8.2		9.1			11.3		18.8			
Δ^4A (ng/mL)		0.5			1.1		1.2						0.6			0.7		2.4	2.9
T (ng/mL)	hCG[g]	2.9	1.6		2.2		4.0		2.6	7.2	1.4	7.9		0.6	3.6	2.4		3.2	9.7
DHT (ng/mL)		0.4			0.2													0.4	1.2
Inhibin B (pg/mL)		61.6			74.6		83.5		75.2										
E_1 (pg/mL)		157			120		124						57			63		53	
E_2 (pg/mL)		29	15		22		59		56		38		24	19		25		58	
E_2/T ratio ($\times 10^3$)		10.0	9.4		10.0		14.8		21.5		27.1			31.7		10.4		18.1	

(b)

Family		Family F								Family G		Family H		Sporadic	
Mutation types		Deletion								Inversion		Inversion		Inversion	
The promoter involved in *CYP19A1* overexpression		*DMXL2*								*CGNL1*		*MAPK6*		*TMOD3*	*TLN2*
Case		Case 11	Case 12	Case 13	Case 14	Case 15	Case 16	Case 17	Case 18	Case 19	Case 20	Case 21[j]		Case 22	Case 23
Age at examination (year)		69	35	44	45	9	8	13	10	35	7	13		17	36
<Phenotypic findings>															
Gynecomastia (tanner breast stage)		**Yes**[i]	**Yes**[i]	**Yes**[i]	**Yes**[i]	**2**	**3**	**3**	**3**	**Yes**	**3**	**5**		N.E.	**Yes**
Onset of gynecomastia (year)		?	?	?	?	**8**	**8**	**11**	**10**	**5**	**5**	**8**		**7**	?
Mastectomy (year)		**Yes**[i]	**Yes**[i]	**Yes**[i]	**Yes**[i]	No	No	**Yes (?)**	**Yes (?)**	**Yes (16)**	No	**Yes (?)**		**Yes (?)**	**Yes (19)**
Testis (ml)		N.E.	N.E.	N.E.	N.E.	2	1.5	**2**	2	N.E.	N.E.	N.E.		Normal	N.E.
Pubic hair (tanner stage)		N.E.	N.E.	N.E.	N.E.	1	1	2	1	Normal	1	**2-3** (at 21.0)		N.E.	N.E.
Facial hair		N.E.	N.E.	N.E.	N.E.	Absent	Absent	Absent	Absent	**Absent**	Absent	N.E.		**Scarce**	N.E.
Height (SDS)[a]		N.E.	~ −1.5	~ −1.5	~ −1.5	+1.4	N.E.	**+2.0**	**+2.4**	**Short**	**>+2.5**	−1.6 (at 21.0)		**Short**	N.E.
Bone age (year)[b]		N.E.	N.E.	N.E.	N.E.	**12.5**	**13.0**	**15.0**	14.5 (at 12.5)	N.E.	**13.0 (at 5.5)**	**17.0**		N.E.	N.E.
Fertility (spermatogenesis)		Yes	Yes	Yes	Yes	?	?	?	?	Yes	?	?		?	?
<Endocrine findings>[c]		B	B	B	B	B	B	B	S	B	B	B	S	B	
<At Dx>	Stimulus														
LH (mIU/mL)	GnRH[e]	**0.2**	3.5	1.7	3.0	0.2	<0.1	2.6	6.3	1.5	1.7	0.1	2.6	**10.0**	4.3
LH (mIU/mL)	GnRH (after priming)[f]														
FSH (mIU/mL)	GnRH[e]	**1.4**	**2.3**	**0.8**	**0.8**	1.4	0.5	**0.8**	**1.2**	**1.2**	**1.5**	0.3	**<0.1**	**<0.1**	**2.7**
FSH (mIU/mL)	GnRH (after priming)[f]														
Prolactin (ng/ml)															
Δ^4A (ng/mL)		1.4	**0.4**	1.7	**0.5**	0.3	<0.3	**0.9**	1.5	1.3	**0.8**	0.3	2.4	**0.9**	
T (ng/mL)	hCG[g]	**2.6**	**2.5**	**2.1**	**2.5**	<0.1	<0.1	**2.7**	9.2	**2.7**	3.2	<0.1	**1.2**	3.8	**2.3**
DHT (ng/mL)													0.2	0.5	
Inhibin B (pg/mL)															
E_1 (pg/mL)		32	34	59	34	26	41	77		86	903	119	544		556
E_2 (pg/mL)		10	19	24	31	11	7	25		40	223	15	178		392
E_2/T ratio ($\times 10^3$)		3.8	7.6	11.4	12.4			9.3		14.8	69.6		148.3		170.4

SDS: standard deviation score; Dx: diagnosis; Tx: therapy; LH: luteinizing hormone; FSH: follicle stimulating hormone; Δ^4A: androstenedione; T: testosterone; DHT: dihydrotestosterone; E_1: estrone; E_2: estradiol; GnRH: gonadotropin-releasing hormone; hCG: human chorionic gonadotropin; N.E.: not examined; B: basal; and S: stimulated.

Abnormal clinical findings are boldfaced.

Abnormally low hormone values are boldfaced, and abnormally high hormone values are underlined.

[a]Evaluated by age- and ethnicity-matched growth references; heights ≥+2.0 SD or below ≤ −2.0 SD were regarded as abnormal.

[b]Assessed by the Tanner-Whitehouse 2 method standardized for Japanese or by the Greulich-Pyle method for Caucasians; bone age was assessed as advanced when it was accelerated a year or more.

[c]Evaluated by age-matched male reference data, except for inhibin B and E_1 that have been compared with data from 19 adult males.

[d]Treated with aromatase inhibitors (anastrozole).

[e]GnRH 100 μg/m^2 (max. 100 μg) bolus i.v.; blood sampling at 0, 30, 60, 90, and 120 minutes.

[f]GnRH test after priming with GnRH 100 μg i.m. for 5 consecutive days.

[g]hCG 3000 IU/m^2 (max 5000 IU) i.m. for 3 consecutive days; blood sampling on days 1 and 4.

[h]Although Case 3 has not yet fathered a child, he has normal spermatogenesis with semen volume of 2.5 ml (reference value: >2 ml), sperm count of 105 × 10^6/ml (>20 × 10^6/ml), total sperm count of 262.5 × 10^6 (>40 × 10^6), motile cells of 70% (>50%), and normal morphological sperms 77% (>30%).

[i]These four patients allegedly had gynecomastia that required mastectomy (age unknown).

[j]The sister has macromastia, large uterus, and irregular menses; the parental phenotype has not been described.

The conversion factor to the SI unit: LH 1.0 (IU/L), FSH 1.0 (IU/L), E_1 3.699 (pmol/L), E_2 3.671 (pmol/L), Δ^4A 3.492 (nmol/L), and T 3.467 (nmol/L).

gynecomastia, small testes with fairly preserved masculinization, obvious or relative tall stature in childhood and grossly normal or apparent short stature in adulthood, and age-appropriate or variably advanced bone ages. Blood endocrine studies revealed markedly elevated E_1 values and E_2/T ratios in all cases examined and normal or variably elevated E_2 values. In addition, Δ^4-androstenedione, T, and dihydrotestosterone values were low or normal, and human chorionic gonadotropin (hCG) test indicated normal T responses. Notably, LH values were grossly normal at the baseline and variably responded to GnRH stimulation, whereas FSH values were low at the baseline and poorly responded to GnRH stimulation even after preceding GnRH priming, in all cases examined.

The severity of such clinical phenotypes is primarily dependent on the underlying mechanisms (Table 1). They are obviously mild in the duplication type, moderate in the deletion type, and severe in the inversion type, except for serum FSH values that remain suppressed irrespective of the underlying mechanisms. Likewise, gynecomastia has been reported to be ameliorated with 1 mg/day of aromatase inhibitor (anastrozole) in the duplication and the deletion types and with 2–4 mg/day of anastrozole in the inversion type [4].

5. Expression Pattern of *CYP19A1* and the Chimeric Genes as One Phenotypic Determinant

Phenotypic severity is much milder in the duplication type than in the deletion and the inversion types. This would be explained by the tissue expression pattern of *CYP19A1* and the chimeric genes. Indeed, RT-PCR analysis using normal human tissue samples revealed that *CYP19A1* is expressed only in a limited number of tissues such as placenta, ovary, skin, and fat, while the five genes involved in the formation of chimeric genes are widely expressed with some degree of variation (Figure 3(b)). Therefore, it is likely that the duplication types would simply increase *CYP19A1* transcription in native *CYP19A1*-expressing tissues, whereas the deletion and the inversion types lead to *CYP19A1* overexpression in a range of tissues, because expression patterns of chimeric genes are predicted to follow those of the original genes. Furthermore, it is also likely that the native *CYP19A1* promoter is subject to negative feedback by elevated estrogens [17], whereas such negative feedback effect by estrogen is weak or even absent for the chimeric genes in the deletion and the inversion types.

6. Structural Property of the Fused Exons as Another Phenotypic Determinant

Phenotypic severity is also milder in the deletion type than in the inversion types, despite a similar wide expression pattern of genes involved in the chimeric gene formation (Table 1, Figure 3(b)). In this context, it is noteworthy that a translation start codon and a following coding region are present on exon 1 of *DMXL2* of the deletion type but not on exons 1 of the chimeric genes of the inversion types (Figure 3(a)). Thus, it is likely that *DMXL2/CYP19A1* chimeric mRNAs transcribed by the *DMXL2* promoter preferentially recognize the natural start codon on *DMXL2* exon 1 and undergo nonsense-mediated mRNA decay and that rather exceptional chimeric mRNAs, which recognize the start codon on *CYP19A1* exon 2, are transcribed into CYP19A1 protein. By contrast, such a phenomenon would not be postulated for the inversion-mediated chimeric mRNAs. Consistent with this, it has been shown that the *DMXL2/CYP19A1* chimeric mRNA is present only in 2–5% of *CYP19A1*-containing transcripts from skin fibroblasts, whereas the *CGNL1/CYP19A1* chimeric mRNA and the *TMOD3/CYP19A1* chimeric mRNA account for 89–100% and 80% of transcripts from skin fibroblasts, respectively [2, 4].

In addition, the genomic structure caused by the rearrangements would affect efficiency of splicing between noncoding exon(s) of neighboring genes and *CYP19A1* exon 2. For example, in the inversion subtype 1, the physical distance between *CGNL1* exon 1 and *CYP19A1* exon 2 is short, and, while a splice competition may be possible between exon 1 of neighboring genes and original *CYP19A1* exons 1, eight of 11 *CYP19A1* exons 1 including exon I.4 have been disconnected from *CYP19A1* coding exons by inversion (Figure 3(a)). This may also enhance the splicing efficiency between *CGNL1* exon 1 and *CYP19A1* exon 2 and thereby lead to relatively severe overexpression of the *CGNL1-CYP19A1* chimeric gene, although this hypothesis would not be applicable for other chimeric genes.

7. Implication for the Hypothalamus-Pituitary-Gonadal Axis Function

It is notable that a similar degree of FSH-dominant hypogonadotropic hypogonadism is observed in the three types, although E_1 and E_2 values and E_2/T ratios are much higher in the inversion type than in the duplication and deletion types (Table 1). In particular, FSH was severely suppressed even after GnRH priming in the duplication type [4]. This implies that a relatively mild excess of circulatory estrogens can exert a strong negative feedback effect on FSH secretion primarily at the pituitary. This would be consistent with the results of animal studies that show strong inhibitory effect of E_2 on transcription of FSH beta-subunit gene in the pituitary cells and almost negligible effect on synthesis of LH beta-subunit and secretion of LH [18, 19]. In this regard, while T responses to hCG stimulation are normal in the duplication and the deletion types and somewhat low in the inversion type, this would be consistent with fairly preserved LH secretion in the three types and markedly increased estrogen values in the inversion type. In addition, whereas fertility and spermatogenesis are normally preserved in the three types, this would be explained by the FSH-dominant hypogonadotropic hypogonadism, because FSH plays only a minor role in male fertility (spermatogenesis) [20].

8. Conclusions

Current studies argue that AEXS is caused by overexpression of *CYP19A1* due to three different types of cryptic genomic rearrangements including duplications, deletions, and inversions. It seems that transcriptional activity and structural property of the fused promoter constitutes the underlying factor for the clinical variability in most features of AEXS except for FSH-dominant hypogonadotropic hypogonadism. Thus, AEXS represents a novel model for gain-of-function mutation leading to human genetic disorders.

References

[1] S. Bhasin, "Testicular disorders," in *Williams Textbook of Endocrinology*, H. M. Kronenberg, M. Melmed, K. S. Polonsky, and P. R. Larsen, Eds., pp. 645–699, Saunders, Philadelphia, Pa, USA, 11th edition, 2008.

[2] M. Shozu, S. Sebastian, K. Takayama et al., "Estrogen excess associated with novel gain-of-function mutations affecting the aromatase gene," *New England Journal of Medicine*, vol. 348, no. 19, pp. 1855–1865, 2003.

[3] M. Demura, R. M. Martin, M. Shozu et al., "Regional rearrangements in chromosome 15q21 cause formation of cryptic promoters for the CYP19 (aromatase) gene," *Human Molecular Genetics*, vol. 16, no. 21, pp. 2529–2541, 2007.

[4] M Fukami, M Shozu, S Soneda et al., "Aromatase excess syndrome: identification of cryptic duplications and deletions leading to gain of function of CYP19A1 and assessment of phenotypic determinants," *The Journal of Clinical Endocrinology & Metabolism*, vol. 96, no. 6, pp. E1035–E1043, 2011.

[5] G. Binder, D. I. Iliev, A. Dufke et al., "Dominant transmission of prepubertal gynecomastia due to serum estrone excess: Hormonal, biochemical, and genetic analysis in a large kindred," *Journal of Clinical Endocrinology and Metabolism*, vol. 90, no. 1, pp. 484–492, 2005.

[6] R. M. Martin, C. J. Lin, M. Y. Nishi et al., "Familial hyperestrogenism in both sexes: clinical, hormonal, and molecular studies of two siblings," *Journal of Clinical Endocrinology and Metabolism*, vol. 88, no. 7, pp. 3027–3034, 2003.

[7] A. Tilpakov, N. Kalintchenko, T. Semitcheva et al., "A potential rearrangement between CYP19 and TRPM7 genes on chromosome 15q21.2 as a cause of aromatase excess syndrome," *The Journal of Clinical Endocrinology & Metabolism*, vol. 90, pp. 4184–4190, 2005.

[8] C. A. Stratakis, A. Vottero, A. Brodie et al., "The aromatase excess syndrome is associated with feminization of both sexes and autosomal dominant transmission of aberrant p450 aromatase gene transcription," *Journal of Clinical Endocrinology and Metabolism*, vol. 83, no. 4, pp. 1348–1357, 1998.

[9] S. Sebastian and S. E. Bulun, "Genetics of endocrine disease: a highly complex organization of the regulatory region of the human CYP19 (Aromatase) gene revealed by the human genome project," *Journal of Clinical Endocrinology and Metabolism*, vol. 86, no. 10, pp. 4600–4602, 2001.

[10] S. E. Bulun, K. Takayama, T. Suzuki, H. Sasano, B. Yilmaz, and S. Sebastian, "Organization of the human aromatase P450 (CYP19) gene," *Seminars in Reproductive Medicine*, vol. 22, no. 1, pp. 5–9, 2004.

[11] M. Demura, S. Reierstad, J. E. Innes, and S. E. Bulun, "Novel promoter I.8 and promoter usage in the CYP19 (aromatase) gene," *Reproductive Sciences*, vol. 15, no. 10, pp. 1044–1053, 2008.

[12] N. Harada, T. Utsumi, and Y. Takagi, "Tissue-specific expression of the human aromatase cytochrome P-450 gene by alternative use of multiple exons 1 and promoters, and switching of tissue-specific exons 1 in carcinogenesis," *Proceedings of the National Academy of Sciences of the United States of America*, vol. 90, no. 23, pp. 11312–11316, 1993.

[13] E. R. Simpson, "Aromatase: biologic relevance of tissue-specific expression," *Seminars in Reproductive Medicine*, vol. 22, no. 1, pp. 11–23, 2004.

[14] E. E. Wallach and C. R. Garcia, "Familial gynecomastia without hypogonadism: a report of three cases in one family," *The Journal of Clinical Endocrinology and Metabolism*, vol. 22, pp. 1201–1206, 1962.

[15] G. D. Berkovitz, A. Guerami, T. R. Brown, P. C. MacDonald, and C. J. Migeon, "Familial gynecomastia with increased extraglandular aromatization of plasma carbon19-steroids," *The Journal of Clinical Investigation*, vol. 75, no. 6, pp. 1763–1769, 1985.

[16] W. Gu, F. Zhang, and J. R. Lupski, "Mechanisms for human genomic rearrangements," *Pathogenetics*, vol. 1, article 4, 2008.

[17] M. B. Yilmaz, A. Wolfe, Y. H. Cheng, C. Glidewell-Kenney, J. L. Jameson, and S. E. Bulun, "Aromatase promoter I.f is regulated by estrogen receptor alpha (ESR1) in mouse hypothalamic neuronal cell lines," *Biology of Reproduction*, vol. 81, no. 5, pp. 956–965, 2009.

[18] J. E. Mercer, D. J. Phillips, and I. J. Clarke, "Short-term regulation of gonadotropin subunit mRNA levels by estrogen: studies in the hypothalamo-pituitary intact and hypothalamo-pituitary disconnected ewe," *Journal of Neuroendocrinology*, vol. 5, no. 5, pp. 591–596, 1993.

[19] D. C. Alexander and W. L. Miller, "Regulation of ovine follicle-stimulating hormone β-chain mRNA by 17β-estradiol in vivo and in vitro," *Journal of Biological Chemistry*, vol. 257, no. 5, pp. 2282–2286, 1982.

[20] T. R. Kumar, Y. Wang, N. Lu, and M. M. Matzuk, "Follicle stimulating hormone is required for ovarian follicle maturation but not male fertility," *Nature Genetics*, vol. 15, no. 2, pp. 201–204, 1997.

MAMLD1 and 46,XY Disorders of Sex Development

Tsutomu Ogata, M.D.[1] Shinichirou Sano, M.D.[1] Eiko Nagata, M.D.[1] Fumiko Kato, M.D.[2] Maki Fukami, M.D.[2]

[1] Department of Pediatrics, Hamamatsu University School of Medicine, Hamamatsu, Japan
[2] Department of Molecular Endocrinology, National Research Institute for Child Health and Development, Tokyo, Japan

Address for correspondence and reprint requests Tsutomu Ogata, M.D., Department of Pediatrics, Hamamatsu University School of Medicine, 1-20-1 Handayama, Higashi-ku, Hamamatsu 431-3192, Japan (e-mail: tomogata@hama-med.ac.jp).

Semin Reprod Med 2012;30:410–416

Abstract

MAMLD1 (mastermind-like domain containing 1) is a recently discovered causative gene for 46,XY disorders of sex development (DSD), with hypospadias as the salient clinical phenotype. To date, microdeletions involving *MAMLD1* have been identified in six patients, and definitive mutations (nonsense and frameshift mutations that are predicted to undergo nonsense mediated mRNA decay [NMD]) have been found in six patients. In addition, specific *MAMLD1* cSNP(s) and haplotype may constitute a susceptibility factor for hypospadias. Furthermore, in vitro studies have revealed that (1) the mouse homolog is expressed in fetal Sertoli and Leydig cells around the critical period for sex development; (2) transient *Mamld1* knockdown results in significantly reduced testosterone production primarily because of compromised 17α-hydroxylation and *Cyp17a1* expression in Murine Leydig tumor cells; (3) MAMLD1 localizes to the nuclear bodies and transactivates the promoter activity of a non-canonical Notch target gene hairy/enhancer of split 3, without demonstrable DNA-binding capacity; and (4) *MAMLD1* is regulated by steroidogenic factor 1 (SF1). These findings suggest that the *MAMLD1* mutations cause 46,XY DSD primarily because of compromised testosterone production around the critical period for sex development. Further studies will provide useful information for the molecular network involved in fetal testosterone production.

Keywords
- *MAMLD1*
- 46,XY DSD
- hypospadias
- testosterone

MAMLD1 (mastermind-like domain containing, 1), previously known as *CXORF6* (chromosome X open reading frame 6), is a recently discovered gene for 46,XY disorders of sex development (DSD) with abnormal external genitalia, especially hypospadias.[1] After the first report describing *MAMLD1* mutations in human 46,XY DSD, a remarkable progress has been made for *MAMLD1*. Here, we summarize the current knowledge about *MAMLD1*, including some hitherto unreported data.

Cloning of *CXORF6* as a Candidate Gene for 46, XY DSD

A gene for 46,XY DSD has been postulated around *MTM1* for myotubular myopathy on Xq28. Indeed, since genital development is normal in patients with intragenic *MTM1* mutations and invariably abnormal in six patients with microdeletions involving *MTM1* (patients 1–6 in ►**Table 1**),[2–5] this suggests that a gene for sex development resides in the vicinity of *MAM1*, and that loss or disruption of the putative sex development gene results in 46,XY DSD as a consequence of contiguous gene deletion syndrome.

In 1997, Laporte et al[6] identified a protein coding gene *CXORF6* from a 430-kb region deleted in two sporadic cases with myotubular myopathy and 46,XY DSD[2] (►**Fig. 1**). *CXORF6* consists of seven exons, and harbors a protein coding sequence on exons 3–6 that is predicted to produce two proteins of 701 and 660 amino acids because of in-frame alternative splicing with and without exon 4. Furthermore, subsequent studies have shown that *MAMLD1* is located

Issue Theme Normal and Abnormal Sex Development — from Patients to Genes; Guest Editor, Berenice B. Mendonca, M.D., Ph.D.

Copyright © 2012 by Thieme Medical Publishers, Inc., 333 Seventh Avenue, New York, NY 10001, USA. Tel: +1(212) 584-4662.

DOI http://dx.doi.org/10.1055/s-0032-1324725. ISSN 1526-8004.